Context Sensitivity Across Multiple Time and Frequency Scales

Regev, Tamar I.[1,*], Markusfeld Geffen[2], Deouell, Leon Y.[1,2,**], and Nelken, Israel[1,3,**]

[1] Edmond and Lily Safra Center for Brain Sciences, The Hebrew University of Jerusalem, Jerusalem, 9190401, Israel

[2] Dept. of Psychology, The Hebrew University of Jerusalem, Jerusalem, 9190501, Israel

[3] Dept. of Neurobiology, The Hebrew University of Jerusalem, Jerusalem, 9190401, Israel

* Corresponding Author, tamar.regev@mail.huji.ac.il. Current address: MIT Department of Brain and Cognitive Sciences, Cambridge, MA 02139, USA, tamarr@mit.edu.

** Equal contribution for last author

Keywords:

Adaptation; EEG; N1; P2; Auditory frequency; Human auditory cortex; Computational modeling

SUMMARY

Everyday auditory stimuli contain structure at multiple time and frequency scales. Using EEG, we demonstrate sensitivity of human auditory cortex to the content of past stimulation in unattended sequences of equiprobable tones. In 3 experiments including 79 participants overall, we found that at different latencies after stimulus onset, neural responses were sensitive to frequency intervals computed over distinct time scales. To account for these results, we tested a model consisting of neural populations with frequency-specific but broad tuning that undergo adaptation with exponential recovery. We found that the coexistence of neural populations with distinct recovery rates can explain our results. Furthermore, the adaptation bandwidth depends on spectral context – it is wider when the stimulation sequence has a wider frequency range. Our results provide electrophysiological evidence as well as a possible mechanistic explanation for dynamic and multi-scale context-dependent auditory processing in the human cortex.

INTRODUCTION

In order to function efficiently, sensory systems should interpret incoming stimuli in the context in which they are embedded. In the auditory modality, context-dependent processing is evident even in responses to pure tones. For example, pure tone sequences can induce contextual effects on phonetic categorization (Darwin & Sutherland, 1984; Holt, 2005, 2006; Stilp & Assgari, 2019). A prominent example of context effects on auditory-evoked neural responses comes from studies involving a sequence of sounds with some regularity, which is infrequently violated by 'deviant' sounds. Numerous studies using this paradigm show that the neural response to sound depends on preceding statistics of the sequence (Garrido, Sahani, & Dolan, 2013; Herrmann, Henry, Fromboluti, McAuley, & Obleser, 2015; Sussman, 2007; Winkler et al., 2003). The neural mechanisms underlying this context sensitivity are still debated. It has been argued that simple adaptation of frequency-selective neurons contributes but cannot fully explain deviance related responses (Näätänen, Jacobsen, & Winkler, 2005; Taaseh, Yaron, & Nelken, 2011; Winkler, Denham, & Nelken, 2009). While most of these studies concentrate on the responses to deviance, processing of context is important for any stimulus sequence structure and not just for detecting a change.

One way of efficiently representing context is by summary statistics of past stimulation. As the environment constantly changes, estimating summary descriptors dynamically may optimize information transmission to the nervous system (Brenner, Bialek, & De Ruyter Van Steveninck, 2000; Fairhall, Lewen, Bialek, & de Ruyter van Steveninck, 2001). Animal studies using electrophysiology have demonstrated that neuronal input-output functions rescale due to dynamic changes in statistical properties such as the mean (Dahmen, Keating, Nodal, Schulz, & King, 2010; Dean, Robinson, Harper, & McAlpine, 2008; Dunn & Rieke, 2006; Nagel & Doupe, 2006), variance (Blake & Merzenich, 2002; Dahmen et al., 2010; Dunn & Rieke, 2006; Kvale & Schreiner, 2004; Maravall, Petersen, Fairhall, Arabzadeh, & Diamond, 2007; Rabinowitz, Willmore, Schnupp, & King, 2011) or higher order moments (Kvale & Schreiner, 2004) of the stimulus distribution. Humans are able to reliably report the mean of a group of objects (Alvarez, 2011). In audition, this has been shown specifically for pitch of pure tones (Albrecht, Scholl, & Chun, 2012; Piazza, Sweeny, Wessel, Silver, & Whitney, 2013). Behavioral and modelling results further suggest that sound textures are represented by the auditory

system using time-averaged statistics (McDermott, Schemitsch, & Simoncelli, 2013; McDermott & Simoncelli, 2011).

Context integration times vary widely, at least between tens of milliseconds to seconds and even minutes (Fairhall et al., 2001; Khouri & Nelken, 2015). Presumably, this is because the natural auditory environment contains relevant information at all of these time scales. Studies have reported modulation of neural responses corresponding to regularities established across multiple time scales in single A1 neurons in animals (Ulanovsky, Las, Farkas, & Nelken, 2004), human MEG (Maheu, Dehaene, & Meyniel, 2019) or the EEG components MMN and P2 (Costa-Faidella, Grimm, Slabu, Díaz-Santaella, & Escera, 2011). However, all of the above studies concentrated on deviance detection.

We investigated context-dependent auditory processing not involving deviance-detection mechanisms by measuring EEG responses to tone sequences in which all stimuli were equi-probable. First, we address data from the control conditions of two experiments (Experiments 1 and 2) we previously published (Regev, Nelken, & Deouell, 2019). Serendipitously, we observed in these conditions sensitivity of the N1 and P2 event-related EEG potentials to past frequency intervals, calculated across distinct time scales. Here, we used quantitative modelling to estimate the effective time and frequency scales of context-dependent neural processes contributing to N1 and P2 separately. We then designed a new experiment (Experiment 3) to replicate and generalize these results. Additionally, in Experiment 3 we manipulated the overall range of frequencies in the sequences and hypothesized that adaptation bandwidths will depend on spectral context.

RESULTS

In 3 EEG experiments, 79 participants (21, 27 and 31 in Experiments 1, 2 and 3) were presented with sequences of 5 equiprobable pure tones, which they were instructed to ignore while concentrating on a silent film. The specific frequencies varied between block types (Figure 1A-B and Methods). Importantly, the sequences were designed pseudo-randomly by concatenating random permutations of the 5 tones and not allowing tone repetitions. This increased the uniformity of tone occurrences over time. Event-related responses (ERP) were computed for each subject, sequence and tone, contingent on the identity of the preceding

tone in the sequence. We examined the amplitudes of the N1 and P2 auditory-evoked responses.

N1 but not P2 is sensitive to long-term context

Absolute N1 amplitudes increased as a function of the frequency interval between the current tone and overall mean frequency in the sequence. This manifested as a typical inverted U-shape pattern, so that the most negative N1 amplitudes were elicited in response to the most extreme tones and the least negative N1 was elicited by the middle tone (which was also approximately equal to the mean frequency of the sequence). This phenomenon was robust and replicated in all 3 experiments (Figure 1C, E). In contrast, P2 amplitudes did not show sensitivity to the mean sequence frequency (Figure 1D, E). To quantify this effect, we used a linear mixed effects model (LME) including data from all experiments together (Table 1 and Figure 2). The slope of the N1 amplitudes on *Interval-Mean* (the interval between the current tone and the mean sequence frequency, semitones) was significantly different from 0 ($F(1,8952)=70$, $p=6.7E-17$, $d=0.94$, Table 1), while the slope of the P2 amplitudes on *Interval-Mean* was not significantly different from 0 ($F(1,8952)=0.15$, $p=0.7$, $d=-0.04$). The difference between the N1 and P2 slopes for *Interval-Mean* was significantly different from 0 ($F(1,8952)=35.5$, $p=2.6E-09$, $d=0.67$, Table 1, Figure 2 – contrast #3). Linear regression on individual participants followed by second-level analysis at the group level gave similar results (supplementary Figure S1 and Table S1).

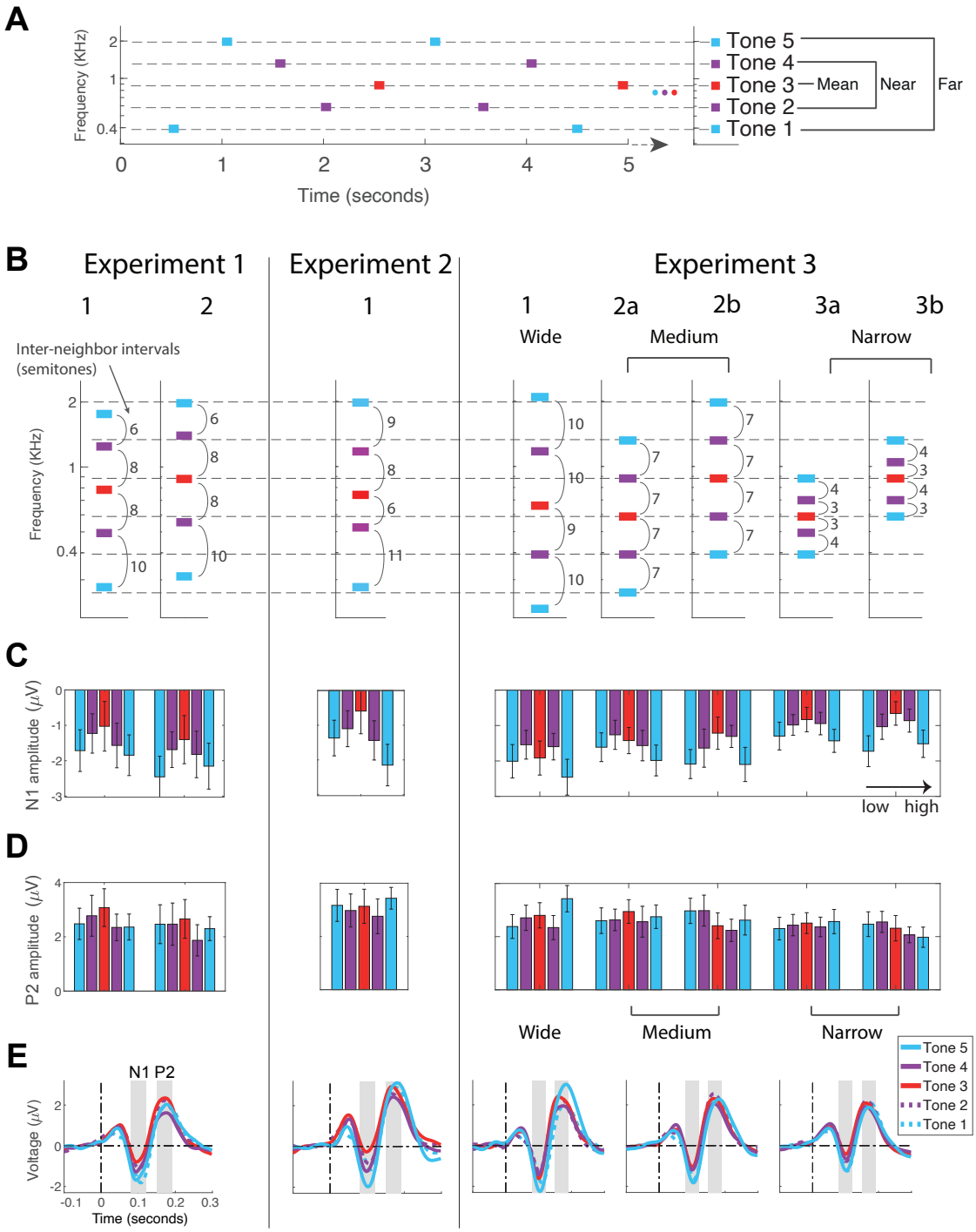

Figure 1 – N1 but not P2 is sensitive to long-term context. A – *An example segment of a tone sequence in the experiment (from block type 2b of Experiment 3).* ***B*** *– Stimuli used in all experiments and conditions. Intervals between neighboring tones on the frequency axis (inter-neighbor intervals) are displayed in semitones.* ***C –*** *Mean and 95% confidence intervals (across participants) of N1 peak amplitudes. For each block type the 5 bars correspond to tones 1, 2, 3, 4 and 5 (lowest to highest) from left to right and the bar colors match the color scheme in panels A and B.* ***D*** *– Same as C for peak amplitude of P2.* ***E*** *– Event-related potentials (ERPs) for tones 1 to 5 (low to high frequency), calculated for each experiment. For Experiment 3, ERPs are plotted for each frequency range, pooling together block types 2a+2b and 3a+3b.*

Table 1 – Linear mixed effects (LME) results - effect of long- and short-term context on N1 and P2. Top *- N1 and P2 amplitudes (standardized using a z-score transform after negating N1 data points) were modeled using the 8 predictors listed in the first (left-most) column. The model consisted of fixed and random factors (grouped by participant) for each of the listed predictors (except for the interaction term Interval-Mean*Interval-Previous which did not have a random factor since the latter did not contribute to explained variance), see Methods. Columns 2 to 5: Fixed-effect estimates (Estimate), standard errors of the estimates (SE), F-statistic used for ANOVA comparing the estimates to 0, with degrees of freedom, significance level (p-value). The predictors Interval-Mean and Interval-Previous stand for the frequency interval between the current tone and sequence mean or current tone and previous tone frequency, respectively, in semitones.* ***Bottom*** *– Post-hoc pairwise coefficient comparison between predictors. The LME model was run on 8960 observations collected from 79 participants overall in the 3 experiments (see methods for elaboration).*

Predictors		**Estimate**	**SE**	**F(1,8952)**	**p-value**	**d**
Intercept	**N1**	-0.51	0.078	42.2	8.8E-11	-0.73
	P2	-0.18	0.074	5.80	0.016	-0.27
Interval-Mean	**N1**	0.04	0.004	70.0	6.7E-17	0.94
	P2	-0.002	0.005	0.15	0.7	-0.04
Interval-Previous	**N1**	0.01	0.003	26.9	2.2E-7	0.58
	P2	0.02	0.003	31.8	1.7E-8	0.63
Interval-Mean * Interval-Previous	**N1**	-0.0008	0.0002	10.08	0.0015	-0.36
	P2	-0.0002	0.0002	0.96	0.32	-0.11

Pairwise comparisons between predictors	**F(1,8952)**	**p-value**	**d**
N1 vs. P2 Interval-Mean	35.5	2.6E-9	0.67
N1 vs. P2 Interval-Previous	0.23	0.62	-0.05
N1 Interval-Mean vs. -previous	25.4	4.6E-7	0.57
P2 Interval-Mean vs. -previous	21.41	3.7E-6	-0.52
N1 Interval-Mean vs. -previous vs. P2 Interval-Mean vs. -previous	46.3	1.03E-11	0.77

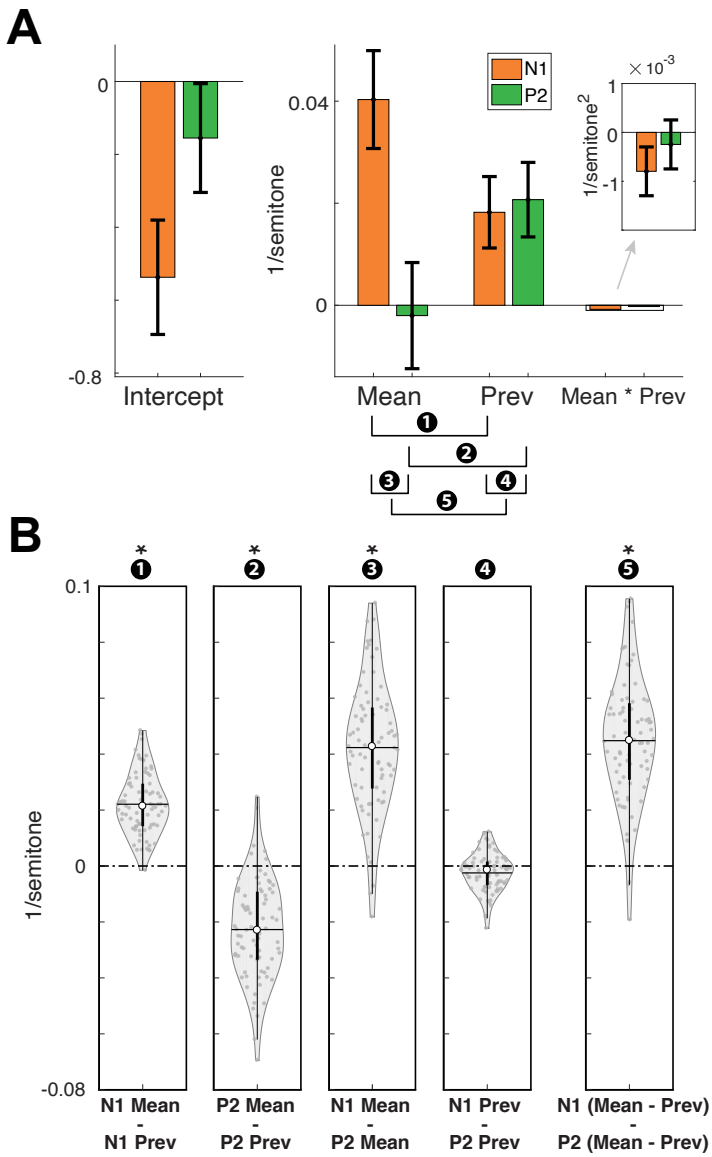

Figure 2 – long- and short-term context effects on N1 and P2 amplitudes. A *– Bar-graphs illustrate fixed-effect estimates values from a linear-mixed effects (LME) model (Table 1 and Methods for further specification). 'Mean' and 'Prev' stand for Interval-Mean and Interval-Previous, denoting the frequency intervals between the current tone and the sequence mean or previous tone, respectively, in semitones. The predicted N1 and P2 voltages were z-scored (after reversing the sign of the N1 data points). Error-bars represent 95% confidence intervals around the estimate (calculated by multiplying the SE of the estimate by the 95% inverse t-distribution value (DF=78)).* ***B*** *–Violin plots illustrate comparisons between LME estimates. Each dot represents one participant. White numbers in black circles above the violin plots indicate to which comparison they correspond (displayed under A). The significant contrasts are marked with an asterisk. Participant-specific estimates were calculated by adding the common fixed-effect estimates to participant-specific random effects. Horizontal lines represent the mean, white circles the medians, and thick and thin black vertical lines represent the 25% and 75% percentiles, respectively.*

P2 is more sensitive than N1 to short-term context

N1 and P2 absolute amplitudes increased as a function of the interval between the current and previous tone frequencies, but this effect was larger for P2 than for N1 (Figure 3). To visualize this, we pooled the possible combinations of current and previous tones according to the 'degree of neighborhood'. Neighbor 1-4 denotes the proximity of tones on the frequency axis in a specific sequence (Figure 3A, B). Figure 3 (C, D) compares the N1 and P2 peak amplitudes for when the previous stimulus was 'Neighbor 1' vs. 'Neighbor 2'. We concentrated just on the 'Neighbor 1' and 'Neighbor 2' groups since they were comprised of more combinations of current and previous tones and included all current tones, whereas by design only extreme tones in every sequence could have neighbor '3' and '4'. The difference between 'Neighbor 1' and 'Neighbor 2' amplitudes was larger for P2 than for N1 in 7 out of 8 block types overall in the 3 experiments (Figure 3D).

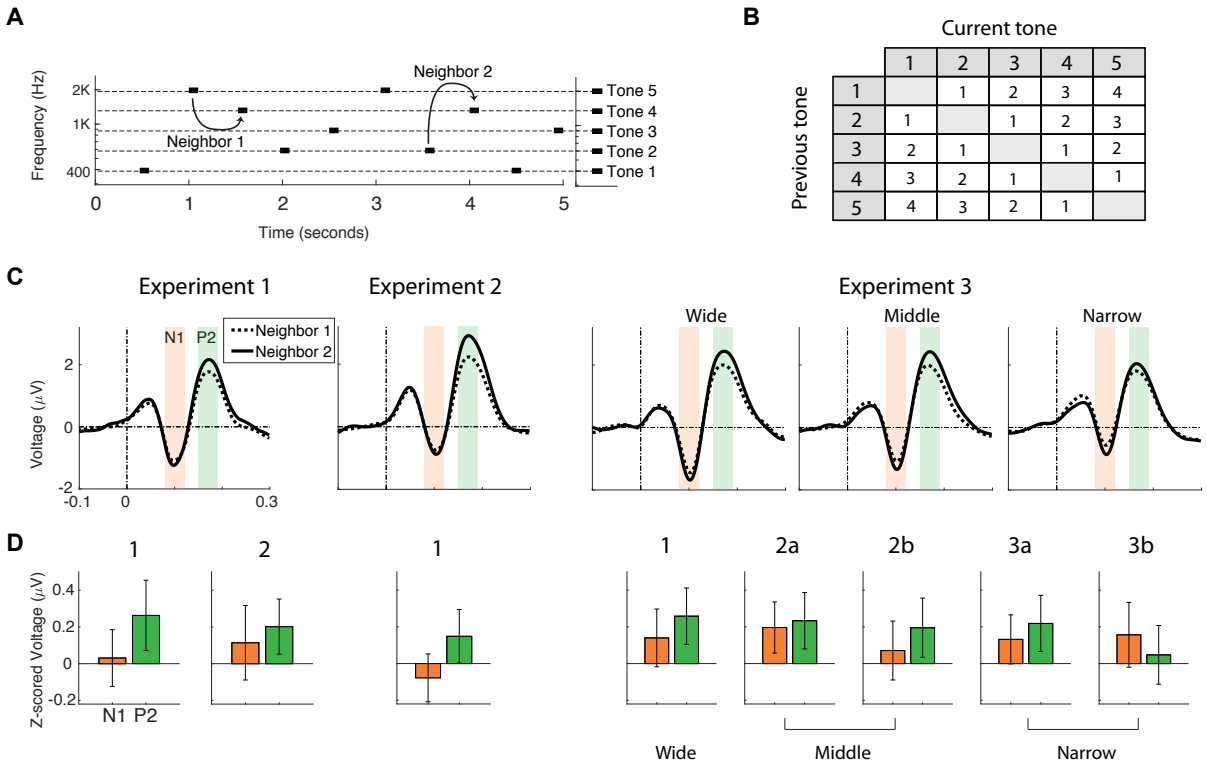

Figure 3 - P2 is more sensitive than N1 to short-term context. A *– Example stimulus sequence denoting one frequency interval between two consecutive tones that are 1st order neighbors on the sequence frequency axis ('Neighbor 1') and the 2nd order neighbors ('Neighbor 2').* ***B*** *– All possible combinations of current and previous tones in a sequence, and their grouping into the 'degree of neighborhood'. Column and row headers of the table denote ordinal tone numbers (1 to 5 from low to high frequencies, see right axis in A). Numbers inside the table denote the 'degree of neighborhood'.* ***C*** *– ERPs of 'current tones' when the previous tone was 'Neighbor 1' and 'Neighbor 2' for each experiment and condition separately. Shaded orange and green areas illustrate the time windows across which the N1 or P2 voltages were averaged.* ***D*** *– Bar-graphs denote the mean and 95% confidence intervals (across participants) of the difference between peak amplitudes in the 'Neighbor 2' and 1' conditions. Peak amplitudes were z-scored for N1 and P2 separately (after reversing the sign of the N1 data points).*

The LME model including data from all experiments together (Table 1, Figure 2) indicated that the frequency interval between the current and previous tone (*Interval-Previous*, semitones) significantly affected both N1 (ANOVA comparing the LME estimates to 0; F(1,8952)=27, p=2.2E-7, d=0.59, Table 1) and P2 (F(1,8952)=31.8, p=1.7E-8, d=0.64) amplitudes. The effect size of *Interval-Previous* was nominally larger for P2 than for N1 but they were not significantly different (F(1,8952)=0.24, p=0.62, d=-0.05). Regressions on individual participants and second-level analysis of regression estimates gave similar results (supplementary Figure S1 and Table S1). Notably, excluding the interaction term from the model reduced the short-

term (Interval-Previous) context effect for N1 but not for P2 (Supplementary Table S2), resulting in a significant difference between N1 and P2 *Interval-Previous* effect (F(1,8954)=9, p=0.0025, d=-0.34). Thus, whereas the dependence of P2 on short-term context was robust, the dependence of N1 on short-term context interacted with its dependence on long-term context.

Sequence frequency range affects N1 but not P2 amplitudes

To test the effect of spectral context on N1 and P2 amplitudes, the overall range of frequencies presented in a sequence was directly manipulated in Experiment 3. Three possible range conditions were tested – Wide, Medium and Small, corresponding to 39, 28 and 14 semitones, respectively, between the lowest and highest tones in each sequence (Figure 1B and Methods). N1 amplitudes were reduced when the frequency range in the sequence was smaller, while P2 amplitudes were not affected much by the frequency range manipulation (Figure 1C and D, Experiment 3), suggesting that N1 amplitudes were more affected by long-term adaptation throughout the sequence than P2. To test this statistically we ran another LME model including *range* as a predictor (Table 2). This analysis confirmed a significant contribution of *range* to the N1 intercept (ANOVA comparing LME estimates to 0; F(1,6188)=36, p=1.9E-9, d=1.1) but not to the P2 intercept (F(1,6188)=1.8, p=0.18, d=0.24) and a significant difference between the effect of range on N1 and P2 intercepts (F(1,6188)=10.9, p=9.5E-4, d=-0.6).

Sequence frequency range interacts with long- and short-term context effect

The same model also indicated that both the short- and long-term context effects were attenuated for sequences with larger frequency ranges, consistent with adaptation with a limited bandwidth. There was a significant interaction between the range and the short-term context variable *Interval-Previous*, such that for both N1 and P2, the effect of *Interval-Previous* was smaller the larger the range was (N1: F(1,6188)=4, p=4.7E-2, d=-0.36), P2: F(1,6188)=6.2, p=1.2E-2, d=-0.46). The interaction between range and the long-term context variable *Interval-Mean* was significant for N1 (F(1,6188)=7.2, p=7.4E-3, d=-0.49, smaller effect of *Interval-Mean* with larger range; Table 2) but not for P2 (F(1,6188)=2.5 p=0.1, d=0.3).

Notably, the interaction terms *interval_mean*interval_previous* did not contribute significantly to this model so we omitted them (see Methods), however see *Supplementary Table S3* for comparison to a model including these terms, which gave similar results.

Table 2 – Linear mixed effects (LME) results including interactions with frequency range. *Entries are similar to Table 1. Here only data from Experiment 3 (31 participants) was used to train the model, resulting in 6200 observations for N1 and P2 altogether (see Methods for an elaboration).*

Predictors		Estimate	SE	F(1,6188)	p-value	d
Intercept	**N1**	-0.76	0.1	55.3	1.2E-13	-1.4
	P2	-0.36	0.1	9.7	1.9E-03	-0.57
Interval-Mean	**N1**	0.054	0.01	17.3	3.2E-05	0.76
	P2	-0.028	0.01	4.2	4.1E-02	-0.37
Interval-Previous	**N1**	0.027	0.009	8.8	3.0E-03	0.54
	P2	0.043	0.009	21.2	4.1E-06	0.84
Range * Intercept	**N1**	0.018	0.003	36.2	1.9E-09	1.1
	P2	0.0041	0.003	1.8	1.8E-01	0.24
Range * Interval-Mean	**N1**	-0.0011	0.0004	7.2	7.4E-03	-0.49
	P2	0.0006	0.0004	2.5	1.1E-01	0.29
Range * Interval-Previous	**N1**	-0.0006	0.0003	4.0	4.7E-02	-0.36
	P2	-0.0007	0.0003	6.2	1.2E-02	-0.46

Comparisons between pairs of predictors	F(1,6186)	p-value	d
N1 vs. P2 (Range * Intercept)	10.9	9.5E-04	0.6
N1 vs. P2 (Range * Interval-Mean)	9.08	2.5E-03	-0.55
N1 vs. P2 (Range * Interval-Previous)	0.13	0.71	0.06

In summary, the ERP results demonstrated that N1 and P2 were affected differently by context: N1 was highly affected by long-term context (*Interval-Mean*) and P2 was not. Additionally, both were affected by short-term context (*Interval-Previous*) but P2 more robustly so. Furthermore, the spectral context (frequency range in the sequence) had a distinct effect on the N1 and P2 amplitudes: smaller sequence range reduced N1 more than

P2 amplitudes, suggesting that adaptation affects the N1 more than it affects the P2. These results imply that N1 and P2 have distinct time scales of contextual influences. Additionally, the effects of long- and short-term context were generally reduced for larger ranges, suggesting that some limited frequency bandwidth plays a role in these effects.

The specific values of the time scales and frequency bandwidth cannot be directly computed using the ERP analysis presented until here. Importantly, the two context predictors we used in the LMEs; *Interval-Mean* and *Interval-Previous* made it possible to consider only very short- (1 previous tone) or very long-term (the sequence mean) contextual effects. In order to estimate the relevant temporal and spectral scales, we employed next a computational model.

Adaptation model

We hypothesized that both the N1 and P2 results could be generated by a single underlying neural mechanism – adaptation of widely tuned frequency-selective neural populations, with two separate time constants.

In the auditory system, frequency-selective neurons respond not only to their characteristic frequency but also to nearby frequencies. Therefore, presenting a tone would adapt not only neural populations tuned exactly to that tone's frequency but also populations tuned to nearby frequencies. Further, if the interval to the next tone is short enough relative to the time scale of adaptation recovery, this adaptation would not recover fully. Thus, given that effective frequency response profiles of neuronal populations are wider than the frequency intervals between tones in a stimulus sequence, cross-frequency adaptation (Taaseh, Yaron, & Nelken, 2011; also termed co-adaptation, Herrmann et al., 2015; Herrmann, Schlichting, & Obleser, 2014) would cause sensitivity of the adapting populations to frequency intervals. Moreover, the time it takes for neurons to recover from adaptation determines the length of temporal accumulation of this effect. If recovery rates are slow relative to the inter-stimulus interval, neurons would accumulate adaptation due to their responses to more than one previous tone in the sequence.

With these premises, we used computational modelling (see Methods for an elaboration) to test the feasibility of adaptation as the neural mechanism accounting for the ERP results

presented above and to estimate quantitatively the effective time and frequency scales underlying the context-sensitivity of the N1 and P2 potentials. A similar modelling approach was applied in the past for neural responses in rats (Taaseh et al., 2011). Further, this model was applied for EEG by Herrmann et al. (2015; 2013; 2014) and we used a similar formulation to the latter studies for comparability. We fitted model predictions to single trial N1 and P2 amplitudes and estimated σ, the bandwidth of frequency response-adaptation profiles, and τ, the time constant of recovery from adaptation (Figure 4A), for N1 and P2 separately.

The adaptation model accounts for N1 and P2 data

The model was fitted to N1 and P2 data separately and the values of $\vec{\theta} = (\sigma, \tau)$ were estimated by selecting the $\vec{\theta}^{max} = (\sigma^{max}, \tau^{max})$ values giving maximum log-likelihood (LL^{max}) model fits, using a search over a pre-determined grid of parameter values. To test the significance of the fit, we fitted the model to surrogate data consisting of random permutations of the measured responses. For both N1 and P2 the LL^{max} values obtained using the actual data were much larger than all null LL^{max} values obtained from the surrogate data. This indicated that the adaptation model fitted the data better than chance ($p<0.004$, since real LL^{max} was larger than all null LL^{max} calculated in 250 repetitions, supplementary Figure S5).

N1 has a longer adaptation recovery time than P2

The estimated time constant for recovery from adaptation, τ^{max}, was consistently longer for N1 relative to P2. This result was found when fitting the model using data from Experiments 1, 2 and 3 separately, as well as when using the data from all experiments together (Figure 4B). The values of τ^{max} were 5, 4.6, 2.4 s (N1) and 0.4, 0.8, 1 s (P2) for Experiments 1, 2, and 3 respectively. It was 3.2 s (N1) and 1 s (P2), when using all data together. In Experiment 1, τ^{max} of N1 was on the upper boundary of the allowed parameter range (5 seconds, equaling 2 repetitions of the 5 stimulus sequence). We limited the τ scale to 5 seconds since the predicted values become almost constant for larger τ values, due to the fact that the stimulus sequence was composed of successive permutations of the five frequencies. Therefore, a time constant of 5 s should be interpreted as 5 or longer.

The difference between τ^{max} of N1 and of P2 was significant. We used three methods for comparing them (see Methods for elaboration): (1) The values of τ^{max} of each potential type fell outside the 95% confidence region of τ^{max} of the other type (Figure 4B); (2) τ^{max} of N1 was larger than τ^{max} of P2 in all bootstrap repetitions we performed (sampling with replacement over the 79 participants and repeating the parameter estimation procedure; Figure 4C, $p<0.01$ since 100 bootstrap repetitions were conducted); and (3) the difference between the log-likelihoods calculated at τ^{max} and at τ^{max} of the other potential type, were significantly larger than their null distribution, estimated by fitting the model to permuted data ($p=0.0039$ for N1 and $p=0.012$ for P2, supplementary Figure S6).

N1 and P2 have similar frequency bandwidths of adaptation

In contrast to the time constant, the estimated frequency bandwidth, σ^{max}, was similar for N1 and for P2. σ^{max} was 10, 7, 8 or 8 semitones for N1 and 4, 9, 9, or 8 semitones for P2 in Experiments 1, 2, 3 or all together, respectively (Figure 4B). In fact, using the data of all experiments together, σ^{max} was exactly 8 semitones for both N1 and P2 (Figure 4B lowest panels). Additionally, the differences between σ^{max} values of N1 and of P2 estimated for 100 bootstrap repetitions of the 79 participants were not significantly different than 0 (Figure 4C).

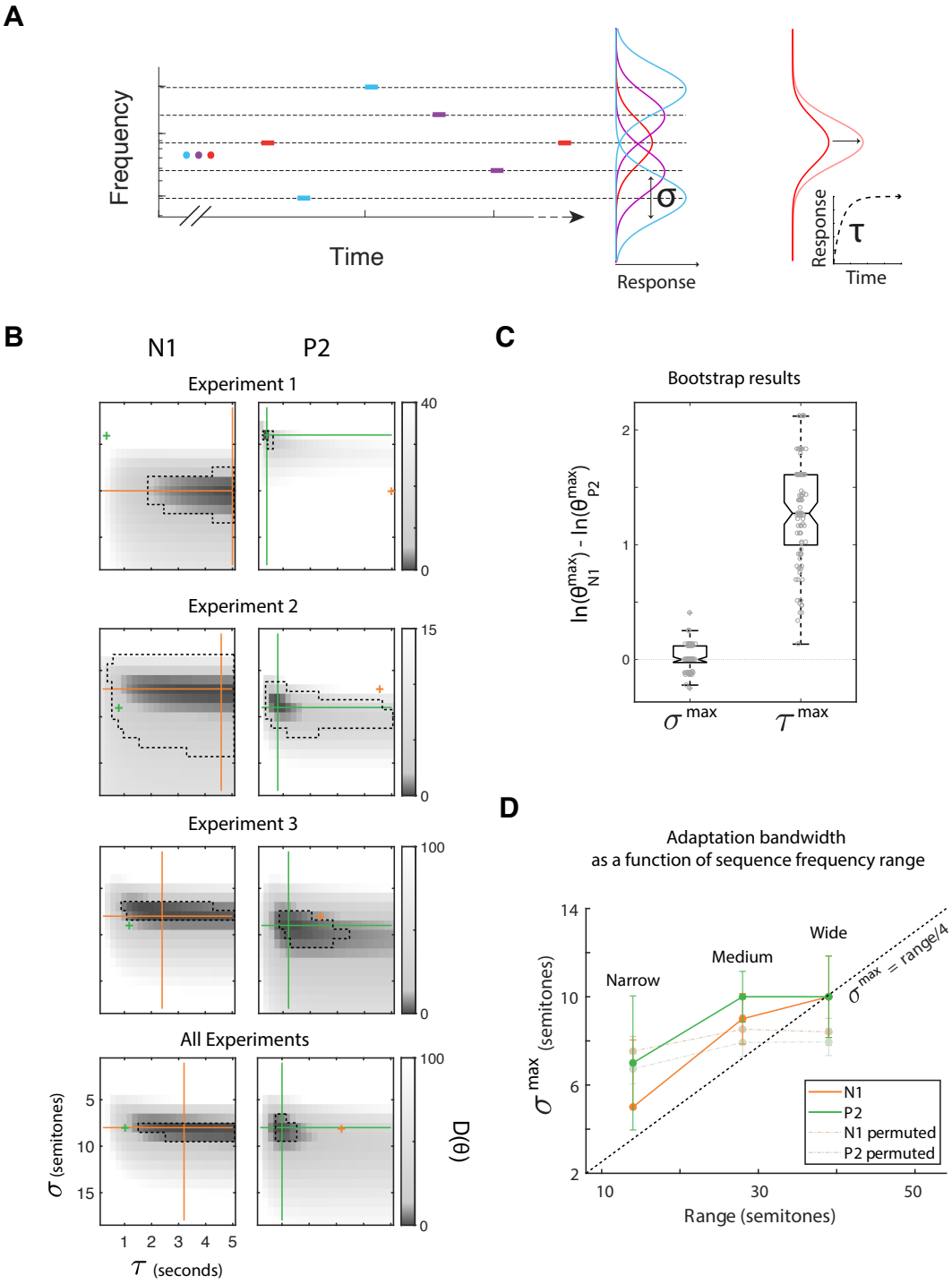

Figure 4 – Adaptation model reveals the time and frequency scales of N1 and P2 context sensitivity. A – Illustration of the adaptation model. Left *– A tone sequence serving as stimulus and schematic Gaussian frequency response-adaptation curves of neural populations assumed by the model, all having the same bandwidth σ. Populations with the red curves respond most frequently throughout the sequence and therefore have the most adapted (attenuated) response profile.* ***Right*** *- Exponential recovery from adaptation. The red curves represent the frequency response of a population at two time points during a period with no tone presentations. Inset below is an exponential recovery curve for a given time constant τ. The response curve*

increases along the arrow connecting the dark to the light red curves, as specified by the exponential function in the inset. ***B, C - N1 and P2 have distinct recovery rates but similar frequency bandwidth. B -*** *D values (-2* log-likelihood ratio relative to $\vec{\theta}^{max}$ which maximizes the likelihood, see Methods), for each possible value of $\vec{\theta} = (\tau, \sigma)$, for each experiment, for N1 (left) and P2 (right). Cross-hairs (N1: orange, P2: green) are located at the maximum-likelihood estimated parameter values (i.e. at $\vec{\theta}^{max}$). Small cross-signs are located at $\vec{\theta}^{max}$ of the other potential type (exactly the crossing point of the neighboring plot, same color code), for visual comparison between $\vec{\theta}^{max}$ of the two potential types. Dashed lines surround 95% confidence regions for $\vec{\theta}^{max}$ calculated according to the null distribution of D (χ^2 with 2 df, see Methods).* ***C -*** *Bootstrap results comparing estimated parameter values for N1 and P2. Each gray dot is the difference between $\vec{\theta}^{max}$ estimated for N1 and for P2 in one of 100 bootstrap repetitions sampling with replacement from the 79 participants and repeating the full parameter estimation procedure.* ***D – Frequency bandwidth depends on spectral context.*** *σ^{max} as a function of stimulus frequency range for N1 (orange), P2 (green) and for N1 and P2 after permuting the order of trials within each range condition 250 times (dashed, see legend). Data from Experiment 3 only. Error bars of the N1 and P2 plots are 95% confidence intervals estimated from 100 bootstrap repetitions sampling with replacement the 31 participants and repeating parameter estimation procedure. Error bars for the permuted data plots are standards errors calculated from the 250 permutations.*

Adaptation bandwidth rescales to the sequence frequency range

Next, we asked whether the parameters of the model (σ^{max} and τ^{max}) are constant when the spectral context changes. We fitted the model and estimated parameter values separately for each of the frequency range conditions in Experiment 3. First, we tested whether allowing the time constant, τ^{max}, to vary for different ranges improves significantly the model fit, but estimating a separate τ did not increase significantly the explained variance neither for N1 (Likelihood ratio test comparing models with constant or varying τ: χ^2=0, df=2, p=1) nor for P2 (χ^2=4.7, df=2, p=0.09). We therefore estimated a single time constant for all the possible ranges. Next, we tested whether the frequency adaptation bandwidth, σ^{max} was constant or differed by spectral context. Estimating a separate σ for each range condition significantly contributed to overall explained variance for N1 (Likelihood ratio test comparing models with constant or varying σ: $\chi^2(2)$=16.4, p=0.0003), but not for P2 ($\chi^2(2)$=1.9, p=0.38). Nevertheless, we decided to fit a model with separate σ^{max} to both the N1 and P2 data for comparison purposes. We found that, interestingly, the values of σ^{max} were consistently close to range/4 (Figure 4D, diagonal dashed line) which is the mean interval between neighboring tones on the sequence-specific frequency axis.

To additionally test whether the modulation of σ by range was significant, we performed 101 bootstrap repetitions (sampling with replacement from the 31 participants) and analyzed the resulting σ^{max} using an LME model (fixed factors: Intercept and range, random factors: Intercept and range grouped by bootstrap number, Methods). Table 3 shows that the dependence of the bandwidth on the range was highly significant with large effect sizes, for both N1 and P2. Thus, although introducing separate bandwidths for the different ranges did not improve the overall fit of the model to the P2 data, nevertheless the bandwidths estimated separately for each range were highly stable. In particular, this test provides evidence that even for the P2 data, the adaptation bandwidth at the smallest range was significantly smaller than at medium and large range.

The dependence of σ^{max} on the stimulus frequency range could potentially be caused merely by an overall reduction of peak amplitudes in sequences with smaller ranges, without any relation to the specific order of the tones in the sequence. To test if this is the case, we permuted the order of data trials within each range condition separately, and repeated the parameter estimation procedure 100 times. The values of σ^{max} obtained using the permuted data showed a slight modulation by frequency range (Figure 4D) but it was not significant (slope of σ^{max} as a function of frequency range estimated for permuted data, N1: 0.04, 95% CI=(-0.03 0.11), not different from 0: t(298)=0.99, p=0.32, P2: 0.05, 95% CI=(-0.02, 0.12), t(298)=1.37, p=0.17). Furthermore, the slopes of σ^{max} as a function of frequency range were significantly larger when using the real and bootstrapped data compared to using the permuted data (Figure 4D) both for N1 (slopes as a function of range: 0.21, 95% CI=(0.19 0.24), note that this confidence region did not overlap with the confidence region of the slope for permuted data presented above) and for P2 (0.13, 95% CI=(0.1 0.15)). Thus, the overall reduction of amplitudes in sequences with smaller ranges was not sufficient to explain the spectral context effect.

Table 3 – LME results – effect of frequency range on adaptation bandwidth. *The data consisted of 101 bootstrap estimates of adaptation bandwidth (sampling with replacement from the 31 participants of Experiment 3 and repeating parameter estimation procedure) for each range condition and potential type (606 data points). The model consisted of fixed and random factors (grouped by bootstrap number) for each of the listed predictors, see Methods.*

Predictors		**Estimate**	**SE**	**F(1,602)**	**p-value**	**d**
Intercept	**N1**	2.7	0.37	52	1.7E-12	0.72
	P2	5.7	0.39	218	2.7E-42	1.5
Range	**N1**	0.22	0.013	283	2E-52	1.7
	P2	0.13	0.013	95	5.8E-21	0.97

DISCUSSION

The two main results reported here demonstrate two forms of context-dependent auditory processing. First, we show distinct patterns of neural sensitivity to the history of stimulation on different time scales, reflected in the event-related N1 and P2 responses. N1 had a longer time scale than P2, such that N1 amplitudes depended on the interval between the current tone and the sequence mean frequency, whereas the P2 amplitudes depended on the interval from the immediately previous stimulus. We show that the results are consistent with a model of adaptation of widely tuned frequency-selective neurons with distinct rates of exponential recovery. Second, the results suggest that adaptation bandwidths dynamically rescale to match the spectral context. In response to sequences of tones with wider frequency distributions and larger frequency intervals, the estimated adaptation tuning width was larger both for N1 and for P2, although the evidence is stronger for N1, implying context-dependent re-organization of auditory representations.

Sensitivity to the mean

Temporal averaging seems to play an important role in perception. The neural mechanism we proposed here might be related to the neural computation of mean across time and its influence on perception. Perception of various modalities was shown over a century ago to contract to the mean over time – subjects tend to underestimate magnitudes larger than the mean, and to overestimate magnitudes smaller than the mean of a given series (Hollingworth, 1910). In the case of tone loudness, it was shown that this memory decay to the mean is correlated to the time constant of MEG habituation effects (Lu & Sperling, 2003; Lu, Williamson, & Kaufman, 1992). In another example, the mean of past interaural-level-differences (ILD) biased judgements in an auditory spatial task (Dahmen et al., 2010). The perceived spatial location was biased away from the mean of preceding stimuli in that study, consistent with adaptation. The ability to perceive the mean of a stimulus distribution is frequently discussed in the context of summary statistics. Humans are able to explicitly report a summary statistic like the mean of a stimulus dimension across multiple stimuli which are distributed not only in space, but also across time. Summary statistics across time has been shown in vision (Albrecht & Scholl, 2010; Haberman, Harp, & Whitney, 2009), for pure tone sequences (Albrecht et al., 2012; Piazza et al., 2013) and as well for implicit representation of

sound textures (McDermott et al., 2013; McDermott & Simoncelli, 2011). The mean can serve as a condensed representation of context.

Our results manifest modulation of neural responses due to the mean of previous stimuli: N1 responses were most adapted for stimuli closest to the mean, consistent with previous reports (Herrmann et al., 2013, 2014; Ulanovsky et al., 2004). We suggest a plausible neural mechanism for computation of the mean across time via continuously summing up the contribution of each stimulus to adaptation at the moment of its occurrence, and gradually forgetting it over time in the form of recovery from adaptation. Effectively, this results in a sliding window (with a length related to the time constant of recovery) in which a sum of all stimuli is computed, with weights that depend on the temporal lag of each stimulus. Behavioral studies employed a similar principle to model a perceptual bias towards the mean of past stimuli, although their model did not explicitly assume neural adaptation. Namely, judgements in a frequency discrimination task were modeled using a Bayesian framework with an exponential decay of single stimulus contributions over time (Raviv, Ahissar, & Loewenstein, 2012). Furthermore, recent stimuli were weighted higher than earlier stimuli to account for the results in a normal population, and this temporal weighting was differentially impaired in several special populations (Lieder et al., 2019). In the case of dyslexics, this perceptual bias to the mean was diminished and the behavioral effect was even correlated to ERP adaptation (Jaffe-Dax, Frenkel, & Ahissar, 2017).

Context integration across several time scales

A central conclusion of the current study is that following the same past sequence of stimulation, brain responses at different latencies are influenced by sequence features that are integrated over distinct time scales. Previous studies demonstrated effects of context at several time scales on neural responses to rare events, including the MMN, (Costa-Faidella et al., 2011), which has both temporal and frontal generators (Deouell, 2007; Giard et al., 1990), potentials in the P3 range (Maheu et al., 2019), having distributed sources including parietal and frontal contributions, as well as frontal and temporal intracranial high frequency broadband activity (Dürschmid et al., 2016). Thus, these studies suggest that neural sources distributed throughout the cortex integrate auditory context at several time scales. The current study adds to this body of literature by providing neural evidence for multiple time

scales of context-dependent processing within human auditory cortex, as well as suggesting a neurally plausible mechanism that is not specifically related to deviance or regularity extraction.

The N1 and P2 auditory evoked potentials were among the earliest recorded human EEG responses (Davis, 1939), but their neural generators and the computations underlying these responses are still not fully understood (Lanting, Briley, Sumner, & Krumbholz, 2013; Picton, 2011). Nevertheless, the neural substrates contributing to the N1 and P2 are thought to reside mainly in auditory cortex. N1 is well-known for being strongly attenuated by stimulus repetition, which was termed either adaptation, habituation or refractoriness (Crowley & Colrain, 2004; Picton, 2011). The effect of stimulus repetition on P2 is more controversial. P2 was sometimes suggested to be less affected by adaptation than N1 (Crowley & Colrain, 2004) and sometime more (Lanting et al., 2013). We demonstrate here that both of these responses show adaptation, but with different recovery rates. This might solve some of the inconsistencies in the literature. Our results contribute to characterizing the functional distinction between these responses and thus support the claim that they are generated by distinct neural populations (Hari, Kaila, Katila, Tuomisto, & Varpula, 1982; Knight, Hillyard, Woods, & Neville, 1980; Lanting et al., 2013).

Estimated recovery rates for N1 were larger than for P2 by at least a factor of 3 (more than 3 seconds for N1 and 1 second or less for P2). Integration over windows of more than 3 seconds allowed calculation of the mean sequence frequency (for N1) whereas less than a second allowed only for sensitivity to 1 or 2 recent stimuli (for P2). These results emphasize that a careful consideration of the specific time constant in adaptation models is essential since different time constants result in qualitatively distinct response properties. In a series of studies, Herrmann et al. (2015, 2013, 2014) used a similar modelling approach to ours, but since they were not particularly interested in the time scale of processing, they fixed the values of both N1 and P2 time constants to 1.8 seconds, based on Sams et al. (1993). Their results were similar to ours for N1 but not for P2 – P2 did not fit well the adaptation model (Herrmann et al., 2013). This might be explained by the time constants we found for P2, which were shorter than 1.8s. Note that a 1.8-seconds-long window sums up more than 3 previous stimuli since the SOA was ~0.5s both in Herrmann et al. and our study.

Nonetheless, the specific values of the time constants we report should not be taken as absolute values since they might depend on specifics of the paradigm. Further, the sequences we used did not contain long-term information over time scales longer than about 5 seconds. For this reason, we only tested recovery time constants up to 5 seconds. In several conditions (Experiment 1, Figure 4B, and when estimating adaptation parameters for each range condition separately in Experiment 3, Figure 4D) the time constant estimated for N1 reached the maximal value of 5 seconds. This might indicate that the time constant of N1 is even longer. Other human electrophysiology studies used sequences that contained longer-term structure and reported longer time scales of integration. For instance, Costa-Faidella et al. (2011) found that P2 and the MMN were sensitive both to regularities established across short (< 1 second) and long (~10 seconds) time scales. The long-term sensitivity of the P2 found in that study is not consistent with our results, which show only short time scales for P2. It could be that sequences embedding longer-term structure could reveal longer time scale sensitivity of P2. However, note that the long-term structure in Costa-Faidella et al. was the violation of a globally established regularity. Thus, the reported long-term sensitivity of P2 may reflect higher-level mechanisms such as prediction, whereas the effects we report may be due to lower-level effects of adaptation.

Early processing of long and later processing of short time scales

Interestingly, we found that the earlier component, the N1, had a longer time constant compared to the P2, which peaks on the scalp later. Similarly, early auditory processing of long-scale sequence properties and later processing of short-scale properties was recently reported in a MEG study (Maheu et al., 2019). These results could be somewhat surprising because longer time scales of integration are frequently associated with a higher-level of processing, which is expected to take place later in the processing hierarchy. For example, consistent with this view, studies employing 'global-local' paradigms found that early sensory cortex was sensitive to short-term, local regularities whereas later and more widespread activity was sensitive to long-term regularities (Bekinschtein et al., 2009; Dürschmid et al., 2016). However, the distinction between short- and long-term regularities in the latter studies, established in the context of deviance detection paradigms, are likely to reflect neural mechanisms that are distinct from the ones underlying our results, obtained in a passive paradigm with no regularities or deviance.

Longer time scales of integration do not necessarily reflect a more complex inference or later latencies. One can think of processing scales in terms of resolution, associating a longer scale with coarser resolution and a shorter scale with a higher resolution that allows to process finer details. This view corresponds with theoretical claims such as the frame-and-fill model developed for vision (Bar, 2006; Snyder, Shpaner, Molholm, & Foxe, 2012), or reverse hierarchy theory (Ahissar & Hochstein, 2004; Nahum, Nelken, & Ahissar, 2008). According to this view, we quickly obtain a general gist of the sensory scene at a coarse resolution, making it possible e.g. to form predictions. This entails early long-scale processing. Later on, the perceptual system may gradually resolve the details, according to task demands, implying shorter scales of processing at later stages, consistent with our results.

Frequency bandwidth rescales to spectral range

We found that adaptation bandwidths rescale to the range of frequency distributions in the sequence. Dynamic adjustment of neural input-output functions due to changes in statistical properties of preceding stimulation has been directly shown using neural measurements in animals for various perceptual dimensions (for a review see Wark, Lundstrom, Fairhall, Mombaerts, & Zador, 2007), such as to light intensity (e.g. Dunn & Rieke, 2006), visual motion (Brenner et al., 2000) and to whisker motion in the barrel cortex of the rat (Maravall et al., 2007). In the auditory modality, rescaling of neuronal tuning to varying statistical properties of sounds were reported in the midbrain of birds (Nagel & Doupe, 2006), mammalian inferior colliculus (Dahmen et al., 2010; Dean et al., 2008; Kvale & Schreiner, 2004), primary auditory cortex of ferrets (Rabinowitz et al., 2011), cats (Gourévitch, Noreña, Shaw, & Eggermont, 2009), and alert primates (Blake & Merzenich, 2002)

In humans, Garrido, Sahani & Dolan (2013) recorded MEG responses to pure tone sequences with frequencies drawn from Gaussian distributions with various widths. Consistent with our results, they found that neural responses to extreme tones were larger compared to tones near the center of the distribution, and that this effect increased for a narrower distribution. However, they concentrated on responses to outlier tones that were less probable than others, especially in narrow frequency distributions. In contrast, in our design all tones were equi-probable. Crucially, these authors emphasize that adaptation mechanisms cannot fully account for their results, since the effects persisted (though diminished) even when analyzing

only tones that were not preceded by other tones falling within about an octave around them for about 7 seconds. Our results suggest that adaptation profiles might be as wide as 9 semitones and rescale to the range of recent stimulus distribution. The adjustment of adaptation bandwidth might further contribute to the differences Garrido et al. (2013) observed between narrow and wide contexts.

The close relation we find between the values of estimated bandwidths and the mean interval between neighboring tones on the sequence-specific frequency axis (range/4, Figure 4D), might allude to a possible relation between the adjustment of bandwidth and the stimulus intervals detected by neuronal populations. Similar to us, Herrmann et al. (2013, 2014) reported adjustment of adaptation bandwidth according to the range of stimulus frequencies. However, Herrmann et al. (2014) found that the overall range of frequencies, rather than the size of intervals across the sequence, was the feature driving the results. This observation was only reported for the N1 potential. An interesting open question is whether this is also the case for P2, or whether given its shorter time scale, as we reported here, the P2 adjustment of bandwidth would be driven by a shorter-scale feature such as interval sizes. Although we extend the claim of bandwidth adjustment to the P2 latency, our data does not allow us to compare the effect of range versus past intervals as we did not independently manipulate them.

The dependence of adaptation bandwidth on the stimulation sequence presumably reflects reorganization of sensory processes. The processes documented here are fast: we know that they occur within a minute - the duration of the sequences. Rapid changes in cortical auditory representations were observed in a behavioral context and suggested to be modulated by top-down processes such as attention (Fritz, Shamma, Elhilali, & Klein, 2003). In contrast, since our paradigm was passive the change of bandwidth did not essentially depend on a task, feedback or top-down processing. Thus, we suggest that bandwidth adaptation is an automatic process. As stated above, there is a host of such context-dependent mechanisms in the auditory system, starting as low as the midbrain (the inferior colliculus). The stages at which the processes we describe occur remain to be revealed.

Conclusion

Our results demonstrate context-dependent processing in two ways that might reflect different mechanisms. The first effect is neural sensitivity to past frequency intervals computed across multiple time scales. We propose that this can be explained by neural adaptation of widely-tuned neural populations with distinct recovery rates. The second effect is the rescaling of adaptation bandwidth to the range of past stimulation. This implies dynamic changes of neural representations due to context. The underlying mechanism for this effect is a matter for future investigation.

Acknowledgements

We thank research assistants who aided with EEG data acquisition and preprocessing: Michal Rabinovits, Eden Krispin, Anael Benistri. TIR was supported by the Hoffman Leadership and Responsibility Program at the Hebrew University. LYD was supported by the Israel Science Foundation and Jack H. Skirball research fund. IN was supported by a grant from the Israel Academy of Sciences (390/13) and by AdERC grant 340063 (project RATLAND), and is the Milton and Brindell Gottlieb Chair in Brain Science.

Author contributions

TIR formulated the study, conducted experiments, developed and conducted analysis methods, and wrote the first draft of the paper. GM conducted experiments. IN and LYD jointly supervised the study, and participated in the design of the experiments, formulation and application of analysis methods and writing the paper.

Declaration of interests

The authors declare no competing interests

Data and Code Availability

Data and code are available via Open Science Framework (OSF): http://osf.io/mswhv

METHODS

Participants

Eighty-nine healthy adults participated in all 3 experiments - 25 musicians, 29 musicians, and 35 non-musicians in Experiments 1, 2 and 3, respectively. The reason musicians participated in Experiments 1 and 2 is not relevant to the current study and is explained in (Regev et al., 2019). Participants were recruited from The Hebrew University of Jerusalem, from Bezalel Academy of Arts and Design or the Jerusalem Academy of Music and Dance, and could either receive 40 NIS (~12 US$) per hour or course credit for participation in the experiment. The data of 7 participants (4, 1 and 2 from Experiments 1, 2 and 3, respectively) were excluded due to technical difficulties with the recording or excessive rates of artifacts. The analysis therefore included the data of 82 participants – 21 in Experiment 1 (7 female, mean age = 29.2 years, SD = 9 years), 28 in Experiment 2 (15 female, mean age = 24.6 years, SD = 3.6 years), and 33 participants in Experiment 3 (19 females, mean age = 24.6, SD = 2.9 years old). All participants self-reported normal hearing and no history of neurological disorders. The experiment was approved by the ethical committee of the faculty of social science at The Hebrew University of Jerusalem, and informed consent was obtained after the experimental procedures were explained.

Stimuli and apparatus

In all experiments, participants were seated in a dimly lit, sound-attenuated, and echo-reduced chamber (C-26, Eckel) in front of a 17-inch CRT monitor (100-Hz refresh rate), at a viewing distance of about 90 cm. The screen was concealed by a black cover, with a rectangular window in the middle (14 by 8.5 cm), through which they viewed the visual display. Auditory stimuli were presented through headphones (Sennheiser HD25, having a relatively flat frequency response function in the range of frequencies used in the experiment) that was placed over the EEG cap. The experiment was run using the Psychophysics toolbox (Brainard, 1997) for MATLAB (version 2013b, MathWorks) running on a 32-bit Windows XP system. Auditory stimuli were synthesized using MATLAB. The experiment included only pure tones, each of 100 milliseconds duration with a 30-millisecond-long linear rise and fall ramps. Stimuli were presented at a sound pressure level that was comfortable for the participants.

At the beginning of the experiment each participant adjusted the relative amplitudes of each individual tone, such that all tones had approximately the same subjective loudness.

Experiment design

Participants viewed silent black and white films while tones were presented to them through headphones. The participants could choose either "The Artist" (Michel Hazanavicius, 2011) or "The Kid" (Charlie Chaplin, 1921), both silent movies. The participants were instructed to ignore the sounds. Each tone sequence in all 3 experiments was comprised of 5 pure tones of different sound frequencies. The specific frequencies varied between block types (see Figure 1, upper row, for an illustration of stimuli, and a detailed description below). To create the sequences, random permutations of the 5 tones were concatenated successively. If the first tone of the next random permutation was the same as the last tone of the previous permutation, the order of tones in next permutation was reversed. As a result, the order of the tones was random with three constraints: each tone occurred exactly in 20% of the sound presentations, a repetition of the same frequency never occurred, and two successive presentations of the same tone frequency were separated by no more than 8 other sounds, which increased the uniformity of tone occurrences over time.

Experiment 1

Two block types (control blocks, in which all tones were equiprobable) from Experiment 1 of Regev et al. (2019) were used for the current study. Condition 1 included 5 tones: Db4, B4, G5, Eb6 and A6 (277.2, 493.9, 784, 1244.5 and 1760 Hz, respectively). Hence, the tones spanned $2\frac{2}{3}$ octaves and the inter-neighbor intervals (frequency intervals between adjacent tones on the frequency axis, see Figure 1B) were 10, 8, 8 and 6 semitones from low to high frequency. The mean frequency (computed on the logarithmic frequency axis) was that of G5 – 784 Hz. Condition 2 included: Eb4, Db5, A5, F6 and B6 (311.1, 554.4, 880, 1397 and 1975.5 Hz, respectively). These were similar to the tones in condition 1, but all shifted 2 semitones down. Three blocks of each condition were presented and their order was counterbalanced between participants. Each block included 500 trials, 100 of each specific tone. This resulted in 300 trials for each specific tone in each condition. The tones were presented with an SOA of either 450 or 550 milliseconds, randomly (average SOA was 500 ms). As a result, each block

took 250 seconds, and there were at least 30 seconds of silence between the blocks (at the participant's discretion). See Figure 1B for illustration of stimuli.

Experiment 2

One block type from Experiment 2 of Regev et al. (2019) was used for the current study. This condition included 5 tones with equal probabilities: Db4, C5, F#5, D6 and B6 (277.9, 523.2, 740, 1174.7, and 1975.6 Hz, respectively). Hence, the tones spanned $2\frac{5}{6}$ octaves and the inter-neighbor intervals were 11, 6, 8 and 9 semitones from low to high frequency. The mean frequency (computed on the logarithmic frequency axis) was that of F#5 – 740 Hz. Two blocks of this condition were presented. Each block included 550 trials presented with an SOA of 400 ms. This resulted in 220 trials for each specific tone. Each block took 220 seconds, and there were at least 30 seconds of silence between the blocks (at the participant's discretion). See Figure 1B for illustration of stimuli.

Experiment 3

In this experiment we manipulated the overall range of frequencies in the sequences. Table 1 summarizes all stimulus details in this experiment. Five block types were used. Block 1 with a wide range of frequencies ($3\frac{1}{4}$ octaves between the highest and lowest tone, i.e. 39 semitones), Blocks 2a and 2b with medium range ($2\frac{1}{3}$ octaves, 28 semitones), and blocks 3a and 3b with narrow range ($1\frac{1}{6}$ octaves, 14 semitones). Correspondingly, the average interval between two neighboring tones (inter-neighbor interval) on the sequence-specific frequency axis values were 9.75, 7 and 3.5 semitones in the Wide, Medium and Narrow range conditions. For the Medium and Narrow conditions, we designed 2 different block types (a and b), such that one was a 7 semitones transposition of the other, which allowed us to generalize the results beyond the specific mean or range of frequencies (Figure 1B). Each block type was presented 3 times such that 15 blocks were presented in total during the experiment. The order of the blocks was randomized for each participant separately, avoiding repetitions of the same block type. In every block 540 tones were presented in total, resulting in 324 trials overall per each specific tone in each block type.

The frequencies of all tones were taken from the C major scale, in order to prevent a situation in which one of the tones would become harmonically deviant and therefore result in

stronger ERP responses (Koelsch, 2009; Poulin-Charronnat et al., 2006). The specific frequencies are specified in Table 1.

Table 1 – Description of stimuli in Experiment 3. *Tone properties are listed from low to high.*

Condition	**1 (wide)**	**2a (medium)**	**2b (medium)**	**3a (narrow)**	**3b (narrow)**
Notes	A3, G4, E5, D6, C7	C4, G4, D5, A5, E6	G4, D5, A5, E6, B6	G4, B4, D5, F5, A5	D5, F5, A5, C6, E6
Frequencies (Hz)	220, 392, 659.26, 1174.7, 2093	261.6, 392, 587.33, 880, 1318	392, 587.3, 880, 1318, 1975.5	392, 493.88, 587.33, 698.46, 880	493.88, 698.46, 880, 1046.5, 1318
Inter-neighbor intervals* (low to high, semitones)	10, 9, 10, 10	7,7,7,7	7,7,7,7	4,3,3,4	3,4,3,4
Mean frequency (note, Hz)	F5, 698.46	D5, 587.33	A5, 880	D5, 587.33	A5, 880
Range (octaves)	$3\frac{1}{4}$	$2\frac{1}{3}$	$2\frac{1}{3}$	$1\frac{1}{6}$	$1\frac{1}{6}$
Range (semitones)	39	28	28	14	14
Mean Inter-neighbor interval (semitones)	9.75	7	7	3.5	3.5

**Mean interval between nearby tones on the sequence-specific frequency scale, Figure 1B*

The SOA (stimulus onset asynchrony, i.e., the time interval between the onsets of two consecutive stimuli) was randomly selected from 5 options: 450, 475, 500, 525 or 550 milliseconds. As a result, the duration of each block was about 270 seconds (4.5 minutes), and there were at least 45 seconds of silence between blocks (at the participant's discretion). In total, the EEG was recorded for approximately an hour and a half.

EEG recording and preprocessing

EEG was recorded from 64 pre-amplified Ag/AgCl electrodes using an Active 2 system (BioSemi, the Netherlands), mounted on an elastic cap according to the extended 10-20 system, with the addition of two mastoid electrodes and a nose electrode. Horizontal electrooculogram (EOG) was recorded from electrodes placed at the outer canthi of the right and left eyes. Vertical EOG was recorded from electrodes placed below the center of both

eyes and above the center of the right eye. The EEG signal was sampled at a rate of 512 Hz (24 bits/channel) with an on-line antialiasing low-pass filter set at one fifth of the sampling rate, and stored for offline analysis.

EEG preprocessing was conducted using BrainVision Analyzer 2.0 (Brain Products), and MATLAB (2016b, MathWorks). The following pre-processing pipeline was applied in all experiments: First, since we paused recording during the break between blocks, de-trending was applied using MATLAB, subtracting long-term linear trends from each block, thus zeroing the signal at beginning and end of blocks and avoiding discontinuities at the border between blocks. Then, further pre-processing was done in Analyzer, using the following pipeline: 0.1 Hz high-pass, zero-phase-shift 2nd order Butterworth filter; referencing to the nose electrode; correction of ocular artifacts using independent component analysis (ICA) (Jung et al., 2000) based on typical scalp topography and time course, combined with manual selection of artifact components having a typical eye-generated topography; and finally, discarding epochs that contained other artifacts. The latter part was semi-automatic – first, an algorithm marked artifacts based on predefined criteria: absolute difference between samples > 100 µV within segments of 100 ms; gradient > 50 µV/ms; absolute amplitude > 100 µV; absolute amplitude < 0.5 µV for a duration of more than 100 milliseconds. If an artifact was detected using any of these criteria, an epoch of 200 milliseconds around it was marked. Then we performed visual inspection of all data to remove or add rare artifacts that were missed or marked by mistake. Artifact rejection was performed on 30 Hz low-passed data, causing the artifact rejection process to be blind to high frequency noise, which did not interfere with our analysis. Then, the data was exported from Analyzer to Matlab (prior to the 30 Hz low-pass filter). Finally, using MATLAB, a 1-20 Hz band-pass zero-phase-shift 4th order Butterworth filter was applied to the continuous data, followed by segmentation and averaging.

Data processing

We calculated Event-Related Potentials (ERPs) locked to auditory stimulus presentation. The ERP amplitudes were measured from the midline central Cz electrode. This location was selected because it maximizes the N1 and P2 responses and is typically used to measure these components (e.g. as in Tremblay, Kraus, McGee, Ponton, & Otis, 2001). The data were parsed into segments beginning 100 milliseconds before the onset of tone presentation and ending

400 milliseconds after tone presentation. The average amplitude of the 100 milliseconds pre-stimulus time served as a baseline for amplitude measurements. ERPs were obtained for each participant, by separately averaging trials of every block type and every tone, conditioned on every possible previous tone. This resulted in 5 tones x 4 previous tones x number of block types (2, 1 or 5 in Experiments 1, 2 and 3, respectively) ERPs. Next, we calculated the peak amplitudes of the N1 and P2 components for each ERP yielding 40, 20 or 100 data points per participant (resulting in 840, 540 and 3100 N1 or P2 points) in Experiments 1, 2 and 3 respectively. Overall this resulted in 4480 points for each potential type, or 8960 altogether.

N1 and P2 peak amplitudes were calculated in two stages. First, to minimize misidentification of peaks due to noise, we determined the peak time from the average of all presentations of each tone (i.e. not conditioned on the previous tone frequency) for each block type and participant. The resulting ERPs were based on a large number of trials and had satisfactory signal-to-noise ratio. At this stage, peaks were detected by the following algorithm. First, we defined the N1 latency as the time of the absolute minimum (most negative) in the time window between 50 and 150 milliseconds after stimulus onset and the P2 latency as the time of the absolute maximum in the time window between 130 and 250 milliseconds after stimulus onset. If the peak latencies corresponded to the edge of the corresponding time windows, the participant was excluded from data analysis. In total, 0, 1 and 2 participants were excluded for this reason from Experiment 1, 2 and 3 respectively. In the second stage of peak amplitude calculation, we computed the average voltage in a 12-milliseconds window around the detected peak time for every possible combination of tone frequency with a previous tone frequency. Thus, peak latencies were determined for each tone frequency and block type regardless of previous tones, whereas the peak amplitudes were measured around these latencies, contingent on the previous tones.

Statistical analysis of ERP peak potentials

To test the effect of both long- and short-term context on N1 and P2 peak amplitudes, we used linear mixed effect models (LME). LME were run in Matlab 2016b using the *fitlme* function. To be able to compare between the N1 and P2 amplitudes, the data were standardized using a z-score transform on the N1 and P2 separately, after multiplying N1 data points by -1. N1 and P2 amplitude values were modeled using 8 fixed factor predictors, 4 for

each potential type. The 4 predictors were: an intercept, two continuous slope variables termed: *Interval-Mean* (long-term context: frequency interval between current tone and mean frequency overall in the sequence, semitones), *Interval-Previous* (short-term context: interval between current and previous tone frequencies, semitones) and another slope variable representing interaction between the two latter variables, encoded as their product: *Interval-Mean*Interval-Previous*. Random effect factors were added for all of the 8 fixed factors, grouped by participant number. In general, to determine whether a factor should be part of the model, we compared the two (nested) models trained with and without this specific factor using a likelihood ratio test (matlab *compare* routine). If the two models were significantly different it meant that the variable contributed significantly to the explained variance and if not, it was excluded. Thus, in this model we omitted the random effects of the interaction variables *Interval-Mean*Interval-Previous* (both for N1 and P2) since they did not contribute to the overall explained variance (Likelihood ratio test between the model with and without these factors; p=0.21 Likelihood-ratio=3). This resulted in 6 random effect terms in the LME. Thus, the LME model is described with the following Wilkinson formula (Wilkinson & Rogers, 1973):

$$\begin{aligned} Voltage \sim I(N1) + I(P2) + Dist_{mean} \cdot I(N1) + Dist_{mean} \cdot I(P2) + Dist_{prev} \cdot I(N1) + Dist_{prev} \\ \cdot I(P2) + Dist_{mean} \cdot Dist_{prev} \cdot I(N1) + Dist_{mean} \cdot Dist_{prev} \cdot I(P2) + (I(N1)|s) \\ + (I(P2)|s) + (Dist_{mean} \cdot I(N1)|s) + (Dist_{mean} \cdot I(P2)|s) + (Dist_{prev} \cdot I(N1)|s) \\ + (Dist_{prev} \cdot I(P2)|s) \end{aligned}$$

Where $Voltage$ is either N1 or P2 standardized amplitudes of the responses to a specific tone (given all previous tone possibilities, for each experiment, condition and participant). $I(N1)$ and $I(P2)$ are indicator functions for N1 or P2 (each being 1 when the voltage belongs to the corresponding class and 0 otherwise). They therefore represent separate intercepts for N1 and for P2. $Dist_{mean}$ stands for *Interval-Mean*, $Dist_{prev}$ stands for *Interval-Previous*. For example, $Dist_{prev} \cdot I(N1)$ denotes the $Dist_{prev}$ slope variable contributing to the N1 amplitudes. $(X|s)$ denotes the random variable *X* grouped by participant number. The variable X is always assumed to be normally distributed with a mean of 0, and its variance is estimated from the data. Thus, $(I(N1)|s)$ denotes a subject-specific contribution to the intercept for the N1 measurements; $(Dist_{prev} \cdot I(N1)|s)$ is a subject-specific contribution to the corresponding slope. This LME model was estimated from data points from all 3

experiments together, resulting in 8960 data points overall (see end of first paragraph of *Data Processing* section above), collected from 79 participants.

Note that this is almost identical to modeling each potential type (N1 or P2) separately by: $Voltage \sim I + Dist_{mean} + Dist_{prev} + Dist_{mean} \cdot Dist_{prev} + (I|s) + (Dist\_prev * I|s) + (Dist\_mean \cdot I|s)$.

However, there are some distinctions. For instance, in the way we estimated the model the residual error is calculated overall from all data together and therefore it is more appropriate for statistical comparisons between the estimates of N1 and P2, which was one of our main goals.

For each fixed effect coefficient, a standardized effect size was computed (Cohen's d). Cohen's d for a specific estimate was computed by dividing the estimate by its standard deviation (SD). The SD was calculated from the estimate standard error (SE) provided by fitlme, multiplying it by square-root(DF), considering DF = 78 (number of participants – 1). The significance value of each individual coefficient (ANOVA comparing it to 0) was given by the *fitlme* model output. To statistically compare between the contributions of two (or more) coefficients we ran a coefficient test (F-test) for LME estimates, using the *coefTest* function in Matlab. Cohen's d of these effects was calculated by dividing the square-root of the F value by the square-root of the relevant DF (78).

To ensure the robustness of the results, we also ran a 2-level analysis, commonly used for example to analyze group results in functional MRI studies. A linear regression was run for each participant with regressors similar to the fixed effects above. We then performed a second-level analysis of the estimates using paired t-tests on participant-specific estimate values (see supplementary Figure S1 and Table S1).

To test the interaction of the overall frequency range of tones in the sequence with the effects estimated by the LME analysis described above, we ran another LME model adding interactions with the continuous slope variable *range* (overall frequency range in the sequence, semitones). For each term in the above model we added another interaction term with *range*. This resulted in a large number of variables in the model and therefore we omitted the higher order variables that did not contribute to the overall explained variance, as described above. All random terms including the *range* variable as well as both fixed and

random effects of the *Interval-Mean*Interval-Previous* (with and without *range* interaction) terms did not contribute to the overall explained variance (Likelihood-ratio test between the models with and without all of the latter terms; $p>0.99$, Likelihood-ratio = 12.3) and therefore were omitted from this model. However, since the fixed factors of the interaction terms *Interval-Mean*Interval-Previous* were included in the previous model, we estimated as well a model including these variables and verified that the results were comparable with and without them (supplementary Table S3). This LME model was run only on data points from Experiment 3, in which the range was manipulated, resulting in 6200 data points (see end of first paragraph of *Data Processing* section above) collected from 31 participants. Significance values and effect sizes were calculated similar to the above, using DF=31-1=30.

Single trial EEG amplitude extraction

We calculated single trial EEG amplitudes as the average voltage of a 12-milliseconds-long window centered around the latency of the N1 and P2 as determined by the subject's ERP (i.e. average across trials). After excluding participants with noisy data or without clear N1 or P2 peaks in the average waveform (see methods section *Data Processing* of chapter 2.2.1), the number of participants in experiments 1, 2 and 3 was 21, 27, and 31, respectively, and 79 altogether. After excluding trials with electric artifacts, we were left with 2626, 1090, 7379 observations per participant on average in experiments 1, 2 and 3, respectively (313,366 observations overall were used to train the model). We also fitted the model separately for each of the frequency range conditions in Experiment 3 (Wide: 39, Medium: 28 and Narrow: 14 semitones). The total number of observations used in each of these conditions was 45,714, 91,979 and 91,072, respectively (Recall that there were 2 versions of the Medium and Narrow conditions, Figure 1A, hence the larger number of trials).

Adaptation Model

The model assumes frequency-tuned neural populations with Gaussian response profiles over a log-frequency axis. Populations have resources, which determine the size of the responses and are depleted in proportion to these responses. Therefore, resource depletion causes attenuation of the responses. Between sound presentations, resources recover exponentially with time. The amount of resources that are depleted is termed response adaptation (RA)

following Herrmann et al. (2015, 2013, 2014). The RA values just before the presentation of a tone were calculated recursively for each specific stimulus sequence, trial by trial, using Equation 1.

Equation 1. $$RA_{i,t+1} = \left(RA_{i,t} + (1 - RA_{i,t}) e^{-\frac{1}{2}\left(\frac{\log(f_i)-\log(f_t)}{\sigma}\right)^2} \right) \cdot e^{\frac{-\Delta t_{S_t \to S_{t+1}}}{\tau}} .$$

Here $RA_{i,t}$ is the response adaptation of neural population i centered around frequency f_i, at time step t of the stimulus sequence, in which stimulus S_t with frequency f_t was presented. RA ranges between 0 (no adaptation) and 1 (maximal adaptation) and therefore 1-RA is the amount of available resources, and is therefore proportional to the response of neurons (full adaptation corresponds to minimum responsiveness and vice versa). The Gaussian term determines the amount of response evoked from this population by the stimulus presented at time t, and therefore of additional resource depletion that is determined by the interval between the current tone presented in the sequence and the best frequency of each neural population. $\Delta t_{S_t \to S_{t+1}}$ is the time interval passing between the onset of the stimulus at time step t and the next stimulus at time step t+1. During this time, resources recover and thus RA decreases exponentially. There are two parameters in Equation 1: the Gaussian width of the frequency profiles - σ, and the time constant of the exponential recovery - τ. These were termed together $\vec{\theta} = (\sigma, \tau)$. Once given, Eq. 1 allows the computation of the adaptation level for each neuronal population and at each time point.

Next, the model assumes a linear relationship between the measured EEG data and RA (Equation 2).

Equation 2. $$Voltage = a + b \cdot RA ,$$

where $Voltage$ is the measured EEG amplitude, either N1 or P2, and a and b are the linear factors associating RA and the data. Since RA is defined between 0 and 1, these factors allowed for appropriate scaling and shift to the EEG units of measurement. The inverse relation between RA and the responsiveness of neurons (1-RA) is captured by the values of a and b.

$RA_{i,t}$ was first computed for all the 5 tone frequencies i and all t time steps in a specific sequence. Each participant heard different stimulus sequences and therefore RA was

computed for each participant separately. Then, to predict responses at each time step t, the relevant RA was taken as that of the i corresponding to the currently presented tone, as in Herrmann et al. (2015, 2013, 2014). The last step assumes that EEG responses measured at time step t are dominated by neural population centered around the frequency of the presented stimulus $f_i = f_t$.

The procedure we used was the one used by Hermann et al. (2013, 2014, 2015), and we used it in order to be consistent with them. A more natural procedure would consist of integrating the RA values for all neuronal populations, weighted by their tuning profiles (the response term in Eq. 1). We verified that the two methods are comparable by calculating the full RA predictions, weighted by the tuning profiles, for one specific participant and plotting them against the simplified model. We show that the two models are strongly linearly dependent (supplementary Figure S3).

Model fit and parameter estimation

All data analysis was carried out using Matlab (Matlab 2016b, Mathworks, MA, USA). In total, the model had four free parameters – The two mechanistic parameters $\vec{\theta} = (\sigma, \tau)$, and the linear factors a and b. All parameters were estimated from the data. However, $\vec{\theta}$ and the linear factors were treated differently. $\vec{\theta}$ are the parameters of interest for this study, while the linear factors are 'nuisance' parameters that have to be fitted but are not interpreted. Therefore, fitting the model was done in two steps. First, single-trial model predictions (RA) were calculated for a range of pre-defined possible $\vec{\theta}$ values; 18 values for σ spanning 1 to 18 semitones, and 25 for τ, spanning 0.2 to 5 seconds with 0.2 second steps (resulting in 450 possible $\vec{\theta}$ combinations). Second, for each $\vec{\theta}$, single trial EEG responses were regressed on the computed RA values. In practice, a linear mixed-effects model (LME) was fitted (using Matlab *fitlme*) using RA as a continuous fixed effect with random intercept and slopes grouped by participant (Wilkinson formula (Wilkinson & Rogers, 1973):

$$Voltage \sim 1 + RA + (1|participant) + (RA|participant)).$$

This approach made it possible to estimate participant-specific linear factors while reducing the amount of overfitting that would be generated by estimating the linear factors of each participant separately. Log-Likelihood (LL) statistics of the LME fit were extracted for each

value of $\vec{\theta}$. Then, $\vec{\theta}^{max}$, the $\vec{\theta}$ value resulting in the maximum likelihood LME fit, was selected as the best estimate for the parameters of interest.

Testing significance of model fit

To test whether the adaptation model generally described the data better than chance we repeated the whole procedure of parameter estimation after randomly permuting the order of data trials such that they didn't match the order of model predictions. For permuted data the model was not expected to perform better than chance and therefore this allowed calculation of the distribution of the LL statistic under the null hypothesis of no effect of sequence order. LL values were calculated for all possible $\vec{\theta}$ values after each of 250 permutations, in the same way it was calculated for the real data. In particular we collected the maximum log-likelihood values out of all possible $\vec{\theta}$ values, for each repetition, and plotted the null distributions of maximum LL values. Next, the maximum LL of real data were compared to the null distributions of maximum LL.

Theoretical formulation of confidence regions of estimated parameter values

To calculate a confidence interval around $\vec{\theta}^{max}$, we asked which $\vec{\theta}$ values are significantly different than $\vec{\theta}^{max}$. Due to Wilk's theorem the quantity:

$$D(\vec{\theta}) = -2 \cdot ln\left(\frac{likelihood(\vec{\theta})}{likelihood(\vec{\theta}^{max})}\right)$$

should be distributed as χ^2 with 2 DF under the null hypothesis that $\vec{\theta}^{max}$ does not describe the data better than any other parameter value, and for a big enough sample size. We also verified this assumption empirically, simulating the null distribution of D and showing that it is comparable to χ^2 with 2 DF at 2 representative values of $\vec{\theta}$ for N1 and P2 data (supplementary Figure S4). We thus calculated the D statistic for all possible $\vec{\theta}$ values and asked whether it is significantly large relative to the χ^2 distribution, with 2 df. A large D is expected for $\vec{\theta}$ values that are significantly different from $\vec{\theta}^{max}$. The statistical question of which $\vec{\theta}$ values are significantly different from $\vec{\theta}^{max}$ is equivalent to calculating a confidence

region for $\vec{\theta}^{max}$. The D values at $\vec{\theta}^{max}$ always equal to 0 by definition. The threshold of D<6, which is approximately the value corresponding to a p=0.05 of the χ^2 distribution with 2 DF, was used to define the 95% confidence region around $\vec{\theta}^{max}$.

Statistical comparison of estimated parameter values for N1 and P2

We statistically contrasted the values of $\vec{\theta}^{max}$ estimated for N1 vs. P2 using three methods. First, we compared the $\vec{\theta}^{max}$ values of N1 and of P2 by checking whether the $\vec{\theta}^{max}$ of, e.g. N1, fell outside the confidence region of P2 and vice versa (see previous section). Second, we performed bootstrapping (random sampling with replacement) on the group of 79 participants (using all experiments together), and repeated the whole estimation procedure 100 times. This resulted in an estimate of the real distribution of $\vec{\theta}^{max}$ values. The distribution of differences of $\vec{\theta}^{max}$ values calculated in the same bootstrap run for N1 vs. P2 was compared to 0. Third, we used a permutation approach to create the null distribution. For each trial, we flipped between N1 and P2 with probability 0.5, 250 times. For each iteration, we repeated the estimation procedure and computed the difference between LL at $\vec{\theta}^{max}$ of the two potential types (termed log-likelihood differences, LLD). We thus estimated the null distribution of LLD under the assumption that the parameters of N1 and P2 were identical, and calculated the p-value of the LLD of the actual data by comparing it to the null distribution.

Statistical comparison of estimated parameter values for different range conditions

$\vec{\theta}^{max}$ values were estimated separately for each of the stimulus frequency range conditions (Wide, Medium and Small) in Experiment 3. Parameter estimation was repeated 100 times using a bootstrap procedure – simulating new groups of participants by random sampling with replacement from the pool of 31 participants. To statistically test the effect of frequency range on adaptation bandwidth of N1 and P2 we used a linear mixed effects (LME) ANOVA on the bootstrapped σ^{max} values, using the Matlab *fitlme* and *anova* functions. The bootstrap repetition number was used as the grouping variable for the random effects. The stimulus

frequency range variable was modeled as a continuous fixed effect with random intercept and slope. Thus, the LME model is described with the following Wilkinson formula:

$$\sigma^{max} \sim I(N1) + I(P2) + range \cdot I(N1) + range \cdot I(P2) + (I(N1)|bootN) + (I(P2)|bootN) + (range \cdot I(N1)|bootN) + (range \cdot I(P2)|bootN)$$

Where σ^{max} are the estimated adaptation bandwidths in each of 100 bootstrap runs, in each of the 3 range conditions and both for N1 and P2 data (600 values in total), and *I(N1)* and *I(P2)* are indicator functions for N1 or P2, respectively. Thus, the *I* represent separate intercepts for N1 and P2. *Range* is the overall range of frequencies presented in a sequence, in semitones (so $range \cdot I(N1)$ represents the effect of range on the N1 bandwidths) and *bootN* is the bootstrap run number serving as a grouping variable for the random effects. Effect size was calculated by dividing the estimate by the SE given by the fitlme function and dividing the result by square-root(DF), considering DF=100-1=99 (for 100 bootstrap repetitions).

SUPPLEMENTARY FIGURES AND TABLES

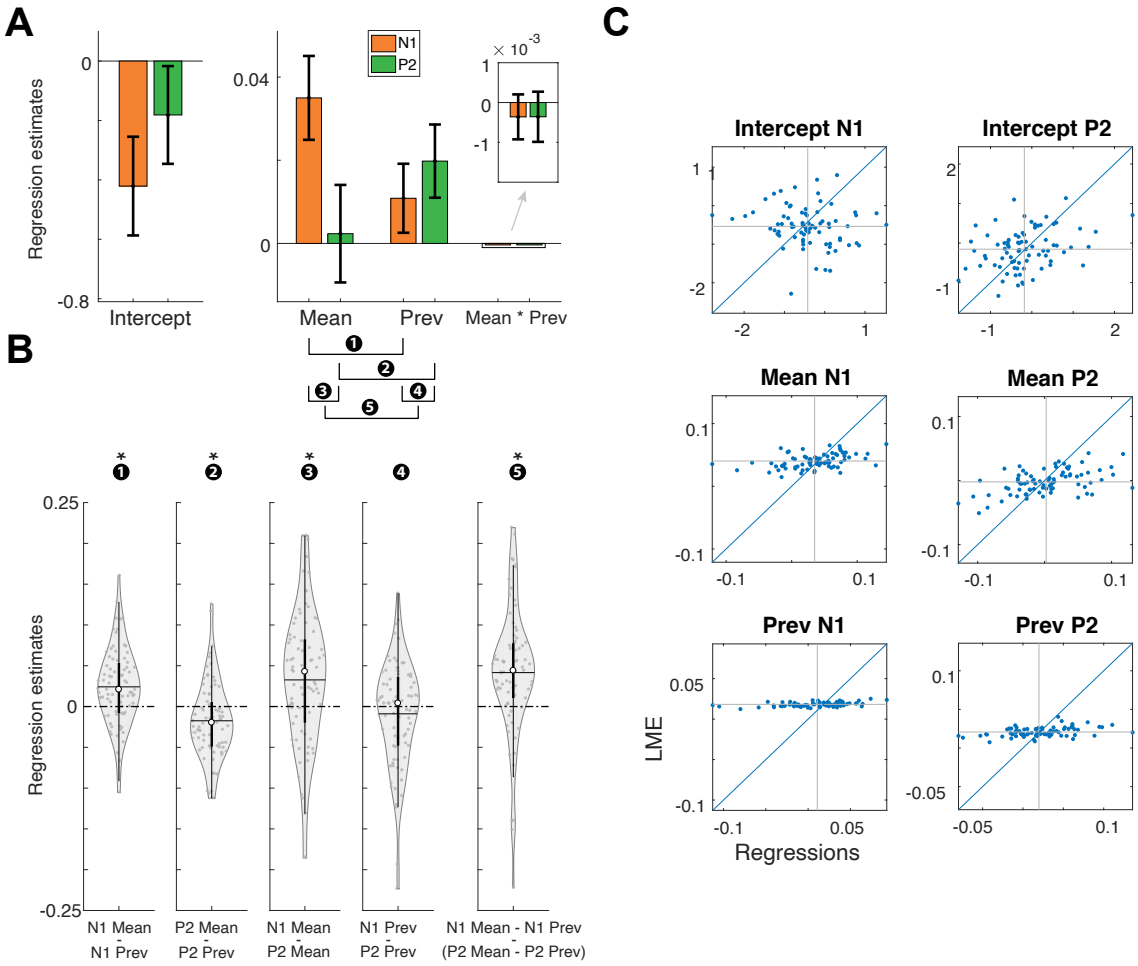

Supplementary Figure S1 – Second-level analysis of the estimates from single-participant regressions. *Compare with the results of the linear mixed effects model (LME) in Figure 2.* ***A*** *and* ***B*** *are the same type of plots as in Figure 2, but using the estimates from single-participant regressions instead of the LME estimates. For the regressions, the same predictors were used as in the fixed factors of the LME. The error bars in A represent the 95% confidence intervals calculated across the group of participant-specific estimates. Each dot in* ***B*** *represents the difference between the relevant estimates per each participant.* Horizontal lines represent the mean, white circles the medians and thick and thin black vertical lines represent the 25% and 75% percentiles, respectively. ***C*** *– Scatter plots of LME vs. regression estimates per participant. Participant-specific estimates in the LME were calculated by adding the common fixed-effect estimate to the participant-specific random estimate. The fact that LME estimates are closer to the mean value than regression estimates illustrates the tendency of the LME to constrain the variability across participants.*

Supplementary Table S1 – Second-level analysis of participant-specific regression estimates, for the long- and short-term context predictors – 'Interval-Mean' and 'Interval-Previous'. *N1 and P2 amplitudes (voltage in μV was standardized using a z-score transform) modeled using the 8 predictors as in Table 1. Here a simple linear regression was run separately for each participant (only fixed, no random factors). For each predictor the estimates for all 79 participants were collected. First row, columns 2 to 5: Estimate – mean estimate across participants. SE – standard error across the group. Cohen's d – mean estimate/SD. P-value – calculated from a t-test comparing the estimate to 0. Five bottom lines refer to a paired t-test comparing between groups of estimates. X vs. Y stands for a subtraction between X and Y. In parenthesis - values from the corresponding LME model (Table 1) for comparison, when relevant.*

Predictors		**Estimate**	**SE**	**t(78)**	**p-value**	**d**
Intercept	**N1**	-0.42 (-0.51)	0.084 (0.078)	-5	2.9E-6 (8.8E-11)	-0.57 (-0.74)
	P2	-0.18 (-0.81)	0.083 (0.074)	-2.2	0.03 (0.016)	-0.24 (-0.27)
Interval-Mean	**N1**	0.035 (0.04)	0.005 (0.004)	7	1.1E-9 (6.7E-17)	0.78 (0.95)
	P2	0.002 (-0.002)	0.006 (0.005)	0.4	0.69 (0.69)	0.04 (-0.04)
Interval-Previous	**N1**	0.01 (0.02)	0.004 (0.004)	2.6	0.01 (2.2E-7)	0.29 (-0.59)
	P2	0.02 (0.02)	0.004 (0.004)	4.4	2.5E-5 (1.7E-8)	0.5 (0.64)
Interval-Mean * Interval-Previous	**N1**	-0.0004 (-0.0008)	0.0003 (0.0002)	-1.2	0.2 (0.001)	-0.14 (-0.36)
	P2	-0.0003 (-0.0002)	0.0003 (0.0002)	-1.1	0.26 (0.33)	-0.12 (-0.11)

Comparisons between pairs of predictors	**t(78)**	**p-value**	**d**
N1 vs. P2 Interval-Mean	3.5	7.1E-4 (2.6E-9)	0.39 (0.67)
N1 vs. P2 Interval-Previous	-1.2	0.21 (0.6)	-0.12 (-0.05)
N1 Interval-Mean vs. -previous	4.5	2.2E-5 (4.7E-7)	0.5 (0.57)
P2 Interval-Mean vs. -previous	-3.3	1.3E-3 (3.7E-6)	-0.37 (-0.52)
N1 Interval-Mean vs. -previous vs. P2 Interval-Mean vs. -previous	4.7	9.4E-6 (1E-11)	0.53 (0.77)

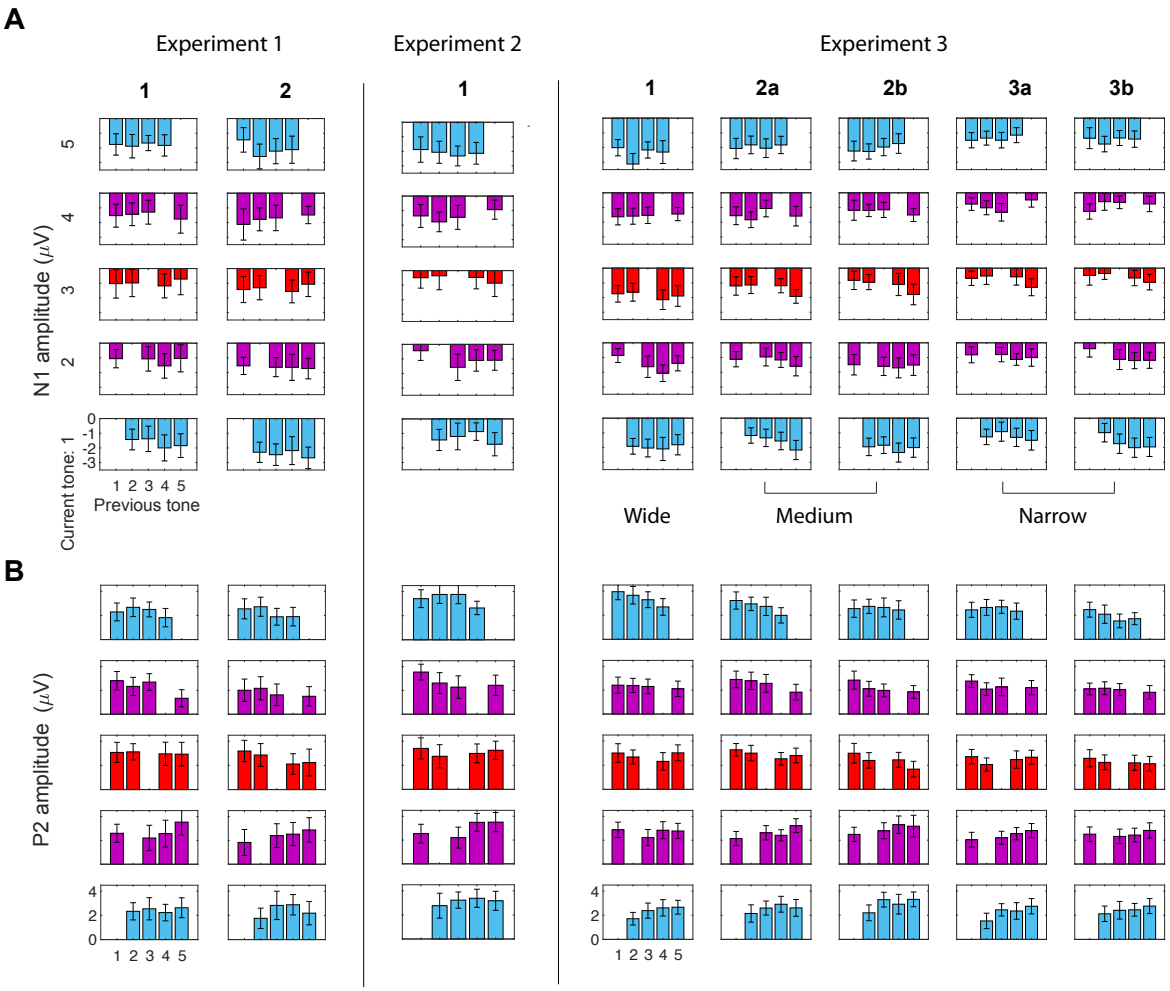

Supplementary Figure S2 – Average N1 and P2 amplitudes, all combinations of current and previous tones. *Bar graphs depict average N1 (**A**) or P2 (**B**) peak amplitudes averaged across participants for every pair of current and previous tones, in every experiment and block type. Error bars represent 95% confidence intervals of the peaks across participants. Numbers under experiment titles denote block types. Tones are ranked from 1 to 5 from low to high frequency, within each block type (as illustrated in Figure 1A). Each row of bar graphs shows the N1/P2 amplitudes for a specific tone rank contingent on the previous tone rank. Since there were no immediate repetitions of the same tone, each graph misses the bar for the immediate repetition (e.g. tone 5 following tone 5 of a sequence, tone 4 following tone 4, etc.). For specific tones' frequencies see Figure 1B and methods.*

Supplementary Table S2 – Linear mixed effects (LME) results for the long- and short-term context predictors – 'Interval-Mean' and 'Interval-Previous', excluding their interaction term*. Entries are similar to Table 1. The actual values of Table 1 (from the LME that included the interaction term) are added in parenthesis for comparison. Note that the main difference between these results and those presented in Table 2 is that in this case the contribution of the short-term context variable (Interval-Previous) to N1 (but not P2) was reduced, and as a result the contrast between Interval-Previous contributions to N1 and P2 is larger and significant (highlighted with underline).*

Predictors		**Estimate**	**SE**	**F(1,8954)**	**p-value**	**d**
Intercept	**N1**	-0.4 (-0.51)	0.07 (0.078)	32.3 (42.2)	1.4E-08 (8.8E-11)	-0.6 (-0.73)
	P2	-0.14 (-0.18)	0.06 (0.074)	4.9 (5.80)	0.028 (0.016)	-0.2 (-0.27)
Interval-Mean	**N1**	0.03 (0.04)	0.003 (0.004)	83 (70.0)	8.2E-20 (6.7E-17)	1 (0.94)
	P2	-0.006 (-0.002)	0.004 (0.005)	2.3 (0.15)	0.13 (0.7)	-0.2 (-0.04)
Interval-Previous	**N1**	0.009 (0.01)	0.002 (0.003)	20.4 (26.9)	6.4E-06 (2.2E-07)	0.5 (0.58)
	P2	0.018 (0.02)	0.002 (0.003)	66 (31.8)	5E-16 (1.7E-08)	0.9 (0.63)

Comparisons between pairs of predictors	**F(1,8954)**	**p-value**	d
N1 vs. P2 Interval-Mean	50 (35.5)	1.9E-12 (2.6E-09)	0.8 (0.67)
N1 vs. P2 Interval-Previous	9 (0.23)	0.0025 (0.62)	-0.34 (-0.05)
N1 Interval-Mean vs. -previous	21 (25)	4.3E-06 (4.6E-07)	0.52 (0.57)
P2 Interval-Mean vs. -previous	23 (21)	1.4E-06 (3.7E-06)	-0.54 (-0.52)
N1 Interval-Mean vs. -previous vs. P2 Interval-Mean vs. -previous	44 (46)	2.9E-11 (1.03E-11)	0.75 (0.77)

Supplementary Table S3 – Linear mixed effects (LME) results including interactions with frequency range and the interaction term Interval-Mean*interval_previous. *This Table is almost identical to Table 2, but the LME model included the interaction terms Interval-Mean * Interval-Previous for N1 and P2. Note that the Interval-Mean * Interval-Previous terms had no significant contribution (highlighted with underline) and therefore were omitted from the LME model reported in Table 2. However, they affected the statistical comparisons between estimates (lower Table). In parenthesis – values from Table 2 (when relevant) for comparison.*

Predictors		Estimate	SE	F(1,6186)	p-value	d
Intercept	**N1**	-0.76 (-0.76)	0.11 (0.1)	52 (55)	6.3E-13 (1.2E-13)	-1.3 (-1.4)
	P2	-0.39 (-0.36)	0.12 (0.11)	10.7 (9.7)	0.001 (0.002)	-0.60 (-0.57)
Interval-Mean	**N1**	0.054 (0.054)	0.01 (0.01)	17.2 (17.3)	3.3E-5 (3.2E-5)	0.76 (0.76)
	P2	-0.029 (-0.028)	0.014 (0.014)	4.5 (4.2)	0.035 (0.041)	-0.39 (-0.37)
Interval-Previous	**N1**	0.027 (0.027)	0.009 (0.009)	8.7 (8.8)	3.2E-3 (3.0E-3)	0.54 (0.54)
	P2	0.042 (0.043)	0.009 (0.009)	19.7 (21.2)	9.0E-6 (4.1E-6)	0.81 (0.84)
Interval-Mean * Interval-Previous	**N1**	0.00002	0.0005	0.0014	0.97	0.01
	P2	0.0005	0.0005	1.3	0.25	0.21
Range * Intercept	**N1**	0.019 (0.018)	0.004 (0.003)	17.5 (36.2)	2.9E-5 (1.9E-9)	0.76 (1.1)
	P2	0.008 (0.0041)	0.004 (0.003)	3.07 (1.8)	0.08 (0.18)	0.32 (0.24)
Range * Interval-Mean	**N1**	-0.0011 (-0.0011)	0.0004 (0.0004)	6.08 (7.2)	0.014 (0.007)	-0.45 (-0.49)
	P2	0.0004 (0.0006)	0.0004 (0.0004)	0.97 (2.5)	0.32 (0.11)	0.18 (0.29)
Range * Interval-Previous	**N1**	-0.0006 (-0.0006)	0.0003 (0.0003)	3.2 (4)	0.073 (0.047)	-0.33 (-0.36)
	P2	-0.0009 (-0.0007)	0.0003 (0.0003)	7.5 (6.2)	6.0E-3 (1.2E-2)	-0.50 (-0.46)

Comparisons between pairs of predictors	F(1,6186)	p-value	d
N1 vs. P2 (Range * Intercept)	2.95 (10.9)	0.086 (0.0009)	0.31 (0.6)
N1 vs. P2 (Range * Interval-Mean)	5.96 (9)	0.015 (0.002)	-0.45 (-0.55)
N1 vs. P2 (Range * Interval-Previous)	0.46 (0.13)	0.5 (0.72)	0.12 (-0.07)

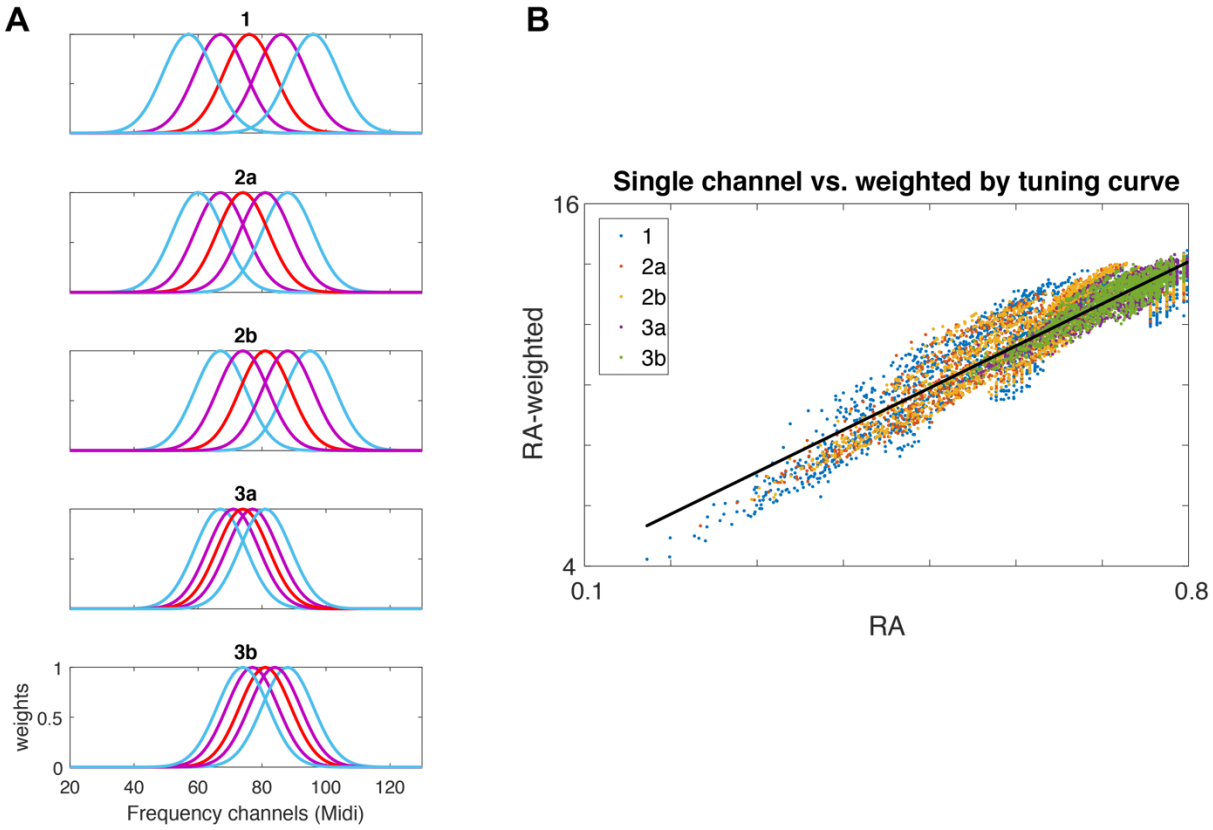

Supplementary Figure S3 – Comparison of RA (the response adaptation model used in this work) to RA weighted by tuning curves. *See Methods for a definition of RA.* ***A*** *– Gaussian tuning curves. Each plot corresponds to a specific block type in Experiment 3 (specified in the titles). In each plot, each Gaussian describes the relevant weights for summing up contributions from neural populations with best frequencies displayed along the x-axis. The 5 Gaussians correspond to the computed responses to each of the 5 tones, color code similar to Figure 1.* ***B*** *– Scatter plot of the weighted RA values (y axis) versus single channel RA values (x axis) as used in this work following* Herrmann et al. (2015, 2013, 2014).

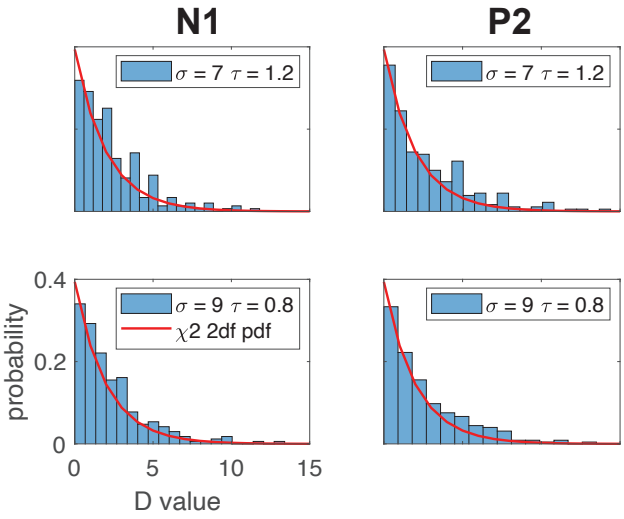

Supplementary Figure S4 – Comparison of the null D distribution to chi-square with 2 degrees of freedom*. Blue - histograms of null D distribution computed for 2 representative values of* $\vec{\theta}$*:* σ *= 7 semitones and* τ *= 1.2 seconds (upper) or* σ *= 9 semitones and* τ *= 0.8 seconds (lower) using N1 (left) or P2 (right) data. Null distribution was simulated by fitting the model to scrambled data, such that the order of data trials did not match that of model predictions, 250 times. The red curve is the theoretical* χ^2 *distribution with 2 degrees-of-freedom.*

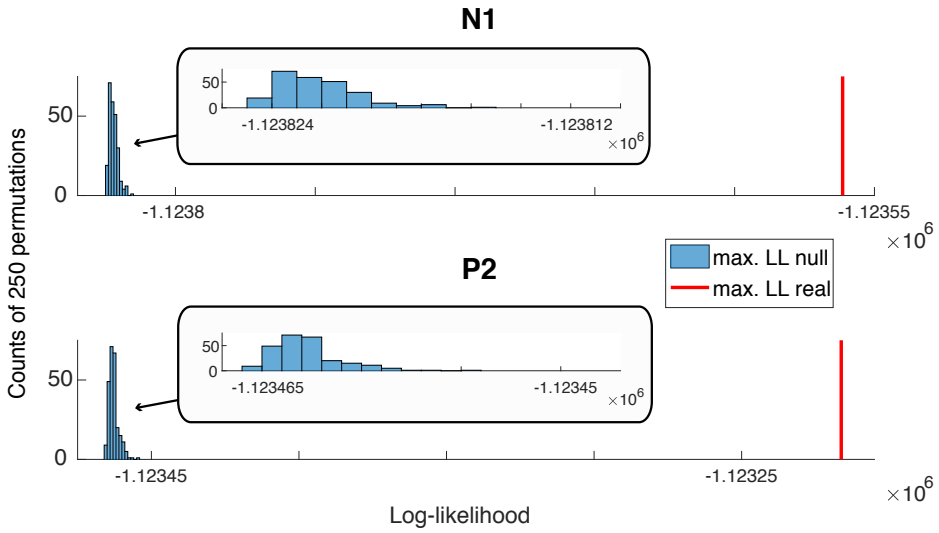

Supplementary Figure S5 – General significance of model fit*.* ***Blue bars*** *- Histograms of null distributions of the maximal Log-Likelihood (LL) of LME model fit. Histograms are constructed using 250 repetitions of model fit after permuting the order of data trials, using the data from all experiments.* ***Red lines*** *– the maximal value of LL out of all tested* $\vec{\theta}$ *values (the LL value at* $\vec{\theta}^{max}$*), when fitting the model using the real (non-scrambled) data.* ***Top –*** *The model fitted to N1 data trials.* ***Bottom –*** *The model fitted to P2 data trials.* ***Insets*** *– Magnifying x-axis values.*

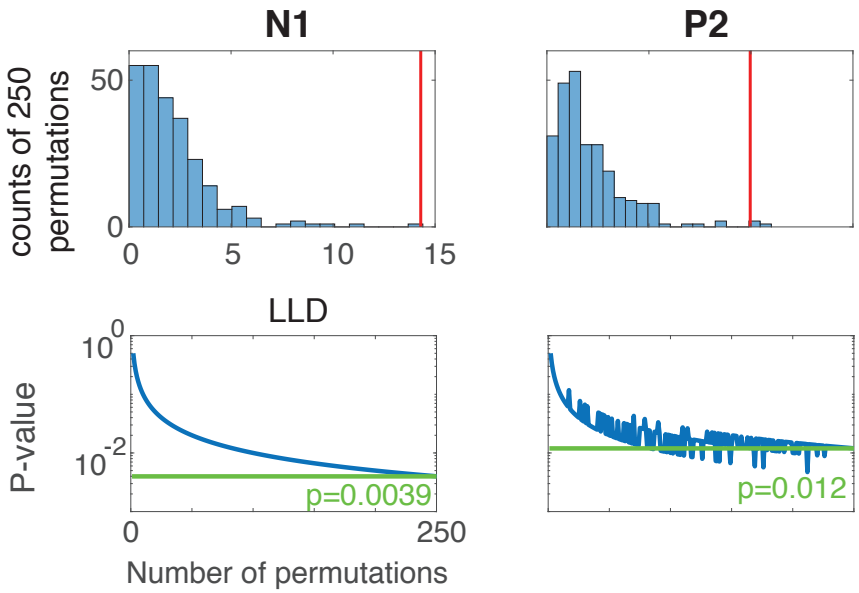

Supplementary Figure S6 – Differences between log-likelihood at τ^{max} and τ^{max} of other potential type (LLD) relative to null distribution. *Null distribution was calculated by fitting the model and estimating parameters for 250 repetitions of random scrambling of data trials such that their order did not match model predictions.* ***Top*** *– blue histograms illustrate the null LLD distribution calculated using the 250 repetitions and red lines indicate the real LLD.* ***Bottom*** *–The green displayed value of p is calculated using all 250 repetitions for the null distribution. The blue line illustrates the p-value as a function of the number of repetitions used (scramble groups are selected randomly from the pool of 250 scramble repetitions calculated). The green line denotes the p-values calculated when using 250 repetitions. Note that the p-values seem to be an upper bound of the real p-value.* ***Left*** *- N1.* ***Right*** *- P2.*

References

Ahissar, M., & Hochstein, S. (2004). The reverse hierarchy theory of visual perceptual learning. *Trends in Cognitive Sciences*, *8*(10), 457–464.

Albrecht, A. R., & Scholl, B. J. (2010). Perceptually Averaging in a Continuous Visual World. *Psychological Science*, *21*(4), 560–567.

Albrecht, A. R., Scholl, B. J., & Chun, M. M. (2012). Perceptual averaging by eye and ear: Computing summary statistics from multimodal stimuli. *Attention, Perception, and Psychophysics*, *74*(5), 810–815.

Alvarez, G. A. (2011). Representing multiple objects as an ensemble enhances visual cognition. *Trends in Cognitive Sciences*, *15*(3), 122–131.

Bar, M. (2006). Top down facilitation of visual recognition. *Proceedings of the National Academy of Sciences of the United States of America*, *103*(36), 449–454.

Bekinschtein, T. A., Dehaene, S., Rohaut, B., Tadel, F., Cohen, L., & Naccache, L. (2009). Neural signature of the conscious processing of auditory regularities. *Proceedings of the National Academy of Sciences of the United States of America*, *106*(5), 1672–1677.

Blake, D. T., & Merzenich, M. M. (2002). Changes of AI receptive fields with sound density. *Journal of Neurophysiology*, *88*(6), 3409–3420.

Brenner, N., Bialek, W., & De Ruyter Van Steveninck, R. (2000). Adaptive rescaling maximizes information transmission. *Neuron*, *26*(3), 695–702.

Costa-Faidella, J., Grimm, S., Slabu, L., Díaz-Santaella, F., & Escera, C. (2011). Multiple time scales of adaptation in the auditory system as revealed by human evoked potentials. *Psychophysiology*, *48*(6), 774–783.

Crowley, K. E., & Colrain, I. M. (2004, April). A review of the evidence for P2 being an independent component process: Age, sleep and modality. *Clinical Neurophysiology*, Vol. 115, pp. 732–744.

Dahmen, J. C., Keating, P., Nodal, F. R., Schulz, A. L., & King, A. J. (2010). Adaptation to Stimulus Statistics in the Perception and Neural Representation of Auditory Space. *Neuron*, *66*(6), 937–948.

Darwin, C. J., & Sutherland, N. S. (1984). Grouping Frequency Components of Vowels: When Is a Harmonic Not a Harmonic? *The Quarterly Journal of Experimental Psychology Section A*, *36*(2), 193–208.

Davis, P. A. (1939). EFFECTS OF ACOUSTIC STIMULI ON THE WAKING HUMAN BRAIN. *Journal of Neurophysiology*, *2*(6), 494–499.

Dean, I., Robinson, B. L., Harper, N. S., & McAlpine, D. (2008). Rapid neural adaptation to sound level statistics. *Journal of Neuroscience*, *28*(25), 6430–6438.

Deouell, L. Y. (2007). The Frontal Generator of the Mismatch Negativity Revisited. *Journal of Psychophysiology*, *21*(3), 188–203.

Dunn, F. A., & Rieke, F. (2006, August 1). The impact of photoreceptor noise on retinal gain controls. *Current Opinion in Neurobiology*, Vol. 16, pp. 363–370. Elsevier Current Trends.

Dürschmid, S., Edwards, E., Reichert, C., Dewar, C., Hinrichs, H., Heinze, H.-J., … Knight, R. T. (2016). Hierarchy of prediction errors for auditory events in human temporal and frontal cortex. *Proceedings of the National Academy of Sciences*, *113*(24), 6755–6760.

Fairhall, A. L., Lewen, G. D., Bialek, W., & de Ruyter van Steveninck, R. R. (2001). Efficiency and ambiguity in an adaptive neural code. *Nature*, *412*(6849), 787–792.

Fritz, J., Shamma, S., Elhilali, M., & Klein, D. (2003). Rapid task-related plasticity of spectrotemporal receptive fields in primary auditory cortex. *Nature Neuroscience*, *6*(11), 1216–1223.

Garrido, M. I., Sahani, M., & Dolan, R. J. (2013). Outlier Responses Reflect Sensitivity to Statistical Structure in the Human Brain. *PLoS Computational Biology*, *9*(3).

Giard, M. -H, Perrin, F., Pernier, J., & Bouchet, P. (1990). Brain Generators Implicated in the Processing of Auditory Stimulus Deviance: A Topographic Event-Related Potential Study. *Psychophysiology*, *27*(6), 627–640.

Gourévitch, B., Noreña, A., Shaw, G., & Eggermont, J. J. (2009). Spectrotemporal receptive fields in anesthetized cat primary auditory cortex are context dependent. *Cerebral Cortex*, *19*(6), 1448–1461.

Haberman, J., Harp, T., & Whitney, D. (2009). Averaging facial expression over time. *Journal of Vision*, *9*(11), 1–1.

Hari, R., Kaila, K., Katila, T., Tuomisto, T., & Varpula, T. (1982). Interstimulus interval dependence of the auditory vertex response and its magnetic counterpart: Implications for their neural generation. *Electroencephalography and Clinical Neurophysiology*, *54*(5), 561–569.

Herrmann, B., Henry, M. J., Fromboluti, E. K., McAuley, J. D., & Obleser, J. (2015). Statistical context shapes stimulus-specific adaptation in human auditory cortex. *Journal of Neurophysiology*, *113*(7), 2582–2591.

Herrmann, B., Henry, M. J., & Obleser, J. (2013). Frequency-specific adaptation in human auditory cortex depends on the spectral variance in the acoustic stimulation. *J Neurophysiol*, *109*, 2086–2096.

Herrmann, B., Schlichting, N., & Obleser, J. (2014). Dynamic Range Adaptation to Spectral Stimulus Statistics in Human Auditory Cortex. *Journal of Neuroscience*, *34*(1), 327–331.

Hollingworth, H. L. (1910). The Central Tendency of Judgment. *The Journal of Philosophy, Psychology and Scientific Methods*, *7*(17), 461.

Holt, L. L. (2005). Temporally Nonadjacent Nonlinguistic Sounds Affect Speech Categorization. *Psychological Science*, *16*(4), 305–312.

Holt, L. L. (2006). The mean matters: Effects of statistically defined nonspeech spectral distributions on speech categorization. *The Journal of the Acoustical Society of America*, *120*(5), 2801–2817.

Jaffe-Dax, S., Frenkel, O., & Ahissar, M. (2017). Dyslexics' faster decay of implicit memory for sounds and words is manifested in their shorter neural adaptation. *ELife*, *6*.

Khouri, L., & Nelken, I. (2015). Detecting the unexpected. *Current Opinion in Neurobiology*, *35*, 142–147.

Knight, R. T., Hillyard, S. A., Woods, D. L., & Neville, H. J. (1980). The effects of frontal and temporal-parietal lesions on the auditory evoked potential in man. *Electroencephalography and Clinical Neurophysiology*, *50*(1–2), 112–124.

Kvale, M. N., & Schreiner, C. E. (2004). Short-Term Adaptation of Auditory Receptive Fields to Dynamic Stimuli. *Journal of Neurophysiology*, *91*(2), 604–612.

Lanting, C. P., Briley, P. M., Sumner, C. J., & Krumbholz, K. (2013). Mechanisms of adaptation in human auditory cortex. *Journal of Neurophysiology*, *110*(4), 973–983.

Lieder, I., Adam, V., Frenkel, O., Jaffe-Dax, S., Sahani, M., & Ahissar, M. (2019). Perceptual bias reveals slow-updating in autism and fast-forgetting in dyslexia. *Nature Neuroscience*, *22*(2), 256–264.

Lu, Z.-L., & Sperling, G. (2003). Measuring Sensory Memory: Magnetoencephalography Habituation and Psychophysics. In *Magnetic Source Imaging of the Human Brain* (pp. 319–342).

Lu, Z. L., Williamson, S. J., & Kaufman, L. (1992). Behavioral lifetime of human auditory sensory memory predicted by physiological measures. *Science*, *258*(5088), 1668–1670.

Maheu, M., Dehaene, S., & Meyniel, F. (2019). Brain signatures of a multiscale process of sequence learning in humans. *ELife*, *8*.

Maravall, M., Petersen, R. S., Fairhall, A. L., Arabzadeh, E., & Diamond, M. E. (2007). Shifts in coding properties and maintenance of information transmission during adaptation in barrel cortex. *PLoS Biology*, *5*(2), 0323–0334.

McDermott, J H, Schemitsch, M., & Simoncelli, E. P. (2013). Summary statistics in auditory perception. *Nature Neuroscience*, *16*(4), 493-U169.

McDermott, Josh H., & Simoncelli, E. P. (2011). Sound texture perception via statistics of the auditory periphery: Evidence from sound synthesis. *Neuron*, *71*(5), 926–940.

Näätänen, R., Jacobsen, T., & Winkler, I. (2005). Memory-based or afferent processes in mismatch negativity (MMN): A review of the evidence. *Psychophysiology*, *42*(1), 25–32.

Nagel, K. I., & Doupe, A. J. (2006). Temporal Processing and Adaptation in the Songbird Auditory Forebrain. *Neuron*, *51*(6), 845–859.

Nahum, M., Nelken, I., & Ahissar, M. (2008). Low-Level Information and High-Level Perception: The Case of Speech in Noise. *PLoS Biology*, *6*(5), e126.

Piazza, E. A., Sweeny, T. D., Wessel, D., Silver, M. A., & Whitney, D. (2013). Humans Use Summary Statistics to Perceive Auditory Sequences. *Psychological Science*, *24*(8), 1389–1397.

Picton, T. W. (2011). *Human Auditory Evoked Potentials*. Plural Publishing.

Rabinowitz, N. C., Willmore, B. D. B., Schnupp, J. W. H., & King, A. J. (2011). Contrast Gain Control in Auditory Cortex. *Neuron*, *70*(6), 1178–1191.

Raviv, O., Ahissar, M., & Loewenstein, Y. (2012). How Recent History Affects Perception: The Normative Approach and Its Heuristic Approximation. *PLoS Computational Biology*, *8*(10), e1002731.

Regev, T. I., Nelken, I., & Deouell, L. Y. (2019). Evidence for Linear but Not Helical Automatic Representation of Pitch in the Human Auditory System. *Journal of Cognitive Neuroscience*, *31*(5), 669–685.

Sams, M., Hari, R., Rif, J., & Knuutila, J. (1993). The Human Auditory Sensory Memory Trace Persists about 10 sec: Neuromagnetic Evidence. *Journal of Cognitive Neuroscience*, *5*(3), 363–370.

Snyder, a C., Shpaner, M., Molholm, S., & Foxe, J. J. (2012). Visual object processing as a function of stimulus energy, retinal eccentricity and Gestalt configuration: a high-density electrical mapping study. *Neuroscience*, *221*, 1–11.

Stilp, C. E., & Assgari, A. A. (2019). Natural speech statistics shift phoneme categorization. *Attention, Perception, and Psychophysics*, *81*, 2037–2052.

Sussman, E. (2007). A New View on the MMN and Attention Debate: The Role of Context in Processing Auditory Events. *Journal of Psychophysiology*, *21*(3–4), 164–175.

Taaseh, N., Yaron, A., & Nelken, I. (2011). Stimulus-Specific Adaptation and Deviance Detection in the Rat Auditory Cortex. *PloS One*, *6*(8), e23369.

Tremblay, K., Kraus, N., McGee, T., Ponton, C., & Otis, B. (2001). Central auditory plasticity: changes in the N1-P2 complex after speech-sound training. *Ear and Hearing*, *22*(2), 79–90.

Ulanovsky, N., Las, L., Farkas, D., & Nelken, I. (2004). Multiple Time Scales of Adaptation in Auditory Cortex Neurons. *Journal of Neuroscience*, *24*(46), 10440–10453.

Wark, B., Lundstrom, B. N., Fairhall, A., Mombaerts, P., & Zador, T. (2007). Sensory adaptation This review comes from a themed issue on Sensory systems Edited Adaptation as efficient coding. *Current Opinion in Neurobiology*, *17*(4), 423–429.

Wilkinson, G. N., & Rogers, C. E. (1973). Symbolic Description of Factorial Models for Analysis of Variance. *Applied Statistics*, *22*(3), 392.

Winkler, I., Denham, S. L., & Nelken, I. (2009, December). Modeling the auditory scene: predictive regularity representations and perceptual objects. *Trends in Cognitive Sciences*, Vol. 13, pp. 532–540.

Winkler, I., Sussman, E., Tervaniemi, M., Horváth, J., Ritter, W., & Näätänen, R. (2003). Preattentive auditory context effects. *Cognitive, Affective and Behavioral Neuroscience*, *3*(1), 57–77.